NASA TECHNICAL MEMORANDUM

NASA TM X-3038

NASA TM X-3038



# AN INLET ANALYSIS FOR THE NASA HYPERSONIC RESEARCH ENGINE AEROTHERMODYNAMIC INTEGRATION MODEL

*by Earl H. Andrews, Jr., James B. Russell, Ernest A. Mackley, and Ann L. Simmonds*

*Langley Research Center*
*Hampton, Va. 23665*

NATIONAL AERONAUTICS AND SPACE ADMINISTRATION • WASHINGTON, D. C. • NOVEMBER 1974

| 1. Report No. | 2. Government Accession No. | 3. Recipient's Catalog No. |
|---|---|---|
| NASA TM X-3038 | | |

| 4. Title and Subtitle | 5. Report Date |
|---|---|
| AN INLET ANALYSIS FOR THE NASA HYPERSONIC RESEARCH ENGINE AEROTHERMODYNAMIC INTEGRATION MODEL | November 1974 |
| | 6. Performing Organization Code |

| 7. Author(s) | 8. Performing Organization Report No. |
|---|---|
| Earl H. Andrews, Jr.; James W. Russell, LTV Aerospace Corporation; Ernest A. Mackley, and Ann L. Simmonds | L-9353 |
| | 10. Work Unit No. |
| | 501-24-16-01 |

| 9. Performing Organization Name and Address | 11. Contract or Grant No. |
|---|---|
| NASA Langley Research Center<br>Hampton, Va. 23665 | |
| | 13. Type of Report and Period Covered |
| 12. Sponsoring Agency Name and Address | Technical Memorandum |
| National Aeronautics and Space Administration<br>Washington, D.C. 20546 | 14. Sponsoring Agency Code |

15. Supplementary Notes

16. Abstract

A theoretical analysis for the inlet of the NASA Hypersonic Research Engine (HRE) Aerothermodynamic Integration Model (AIM) has been undertaken by use of a method-of-characteristics computer program. The purpose of the analysis was to obtain pretest information on the full-scale HRE inlet in support of the experimental AIM program (completed May 1974).

Mass-flow-ratio and additive-drag-coefficient schedules were obtained that well defined the range effected in the AIM tests. Mass-weighted average inlet total-pressure recovery, kinetic energy efficiency, and throat Mach numbers were obtained.

| 17. Key Words (Suggested by Author(s)) | 18. Distribution Statement |
|---|---|
| Inlet<br>Propulsion | Unclassified – Unlimited<br><br>STAR Category 01 |

| 19. Security Classif. (of this report) | 20. Security Classif. (of this page) | 21. No. of Pages | 22. Price* |
|---|---|---|---|
| Unclassified | Unclassified | 44 | $3.25 |

*For sale by the National Technical Information Service, Springfield, Virginia 22151

# AN INLET ANALYSIS FOR THE NASA HYPERSONIC RESEARCH ENGINE AEROTHERMODYNAMIC INTEGRATION MODEL

By Earl H. Andrews, Jr., James W. Russell,*
Ernest A. Mackley, and Ann L. Simmonds
Langley Research Center

## SUMMARY

An inlet theoretical analysis has been conducted in support of the aerothermodynamic research program for the NASA Hypersonic Research Engine (HRE) Project which is scheduled to culminate in an experimental investigation of the Aerothermodynamic Integration Model (AIM)[1] in the Lewis Hypersonic tunnel facility (HTF) at the Plum Brook Station at nominal Mach numbers of 5, 6, and 7. The AIM experimental investigation is for the purpose of determining the net aerodynamic and thermodynamic effects of the three full-scale components (inlet, combustor, and nozzle) when integrated. It is desirable to evaluate the AIM combustor performance; however, the combustor entrance conditions (inlet throat conditions) will not be experimentally obtained from AIM test measurements. Therefore, it was considered necessary to conduct a theoretical analysis of the AIM inlet. A method-of-characteristics computer program was employed to perform the inlet computations (the program can compute for two-dimensional or axisymmetric, real-gas or ideal-gas, supersonic external and internal flows, with or without boundary layer at constant wall temperatures).

The computer program was used for generating a number of cases for various real-gas, viscid-inviscid flow conditions. Ranges of mass-flow ratios and additive drag coefficients for the scheduled AIM test conditions were calculated, and "curve fits" for the mass-flow ratios as a function of cowl position and Mach number were obtained. Mass-weighted average inlet performances – total-pressure recovery, kinetic energy efficiency, and throat Mach number – were also calculated. "Shock-on-lip" total-pressure-recovery results supplemented previously documented sparse HRE full-scale (flight condition) analytical results to the extent that a nearly straight-line decreasing trend was indicated over the free-stream Mach number range from 4 to 8.

---

*LTV Aerospace Corporation, Hampton, Va.

[1]Inlet analysis performed in 1972; AIM tests completed May 1974.

## INTRODUCTION

As part of the NASA Hypersonic Research Engine (HRE) Project, tests of a complete engine (inlet-combustor-nozzle) designated the Aerothermodynamic Integration Model (AIM) are planned. The AIM is a full-scale, water-cooled, boilerplate engine which burns hydrogen fuel. Component tests have been performed on (1) a 2/3-scale inlet model in unheated-air wind tunnels (ref. 1); (2) a two-dimensional combustor model with direct-connect hot vitiated airflow (ref. 2); and (3) a nozzle model with direct-connect cold and hot airflow (ref. 3). Another two-dimensional combustor model, which closely represented a segment of the HRE-AIM annulus combustor, was tested in 1971 (ref. 4). The experimental investigation of the AIM is scheduled to be conducted in the Lewis hypersonic tunnel facility (HTF) at the Plum Brook Station at nominal Mach numbers of 5, 6, and 7 for the purpose of determining the net aerodynamic and the thermodynamic effects of the three components when integrated as a complete full-scale engine.

Inlet throat (combustor entrance) conditions must be known in order to properly evaluate the combustor performance during the AIM experimental investigation. However, direct measurements for determining inlet throat conditions and performance will not be obtained during the AIM tests; surface pressure measurements and calculated skin-friction forces will be used to determine the inlet momentum losses and thus the performance. Therefore, it was considered necessary to theoretically analyze the AIM inlet in order to obtain throat conditions needed for evaluations of the AIM combustor performance and inlet performance values for comparison with those to be obtained during the AIM tests, and to thoroughly map the inlet mass ratios for the AIM test conditions. The need for theoretical inlet mass-flow data became increasingly important when the engine airflow metering tests originally planned had to be abandoned. Some theoretical analyses at Mach 4, 6, and 8 flight conditions were performed for the HRE full-scale inlet and reported in reference 1. The full-scale inlet results of the reference 1 analysis are very sparse and do not well define the range of conditions for the AIM experimental investigation. Therefore, the purpose of the present analysis is to supplement the results of reference 1 so as to have a more thorough inlet analysis for the conditions of the AIM experimental investigation. Such an analysis was performed by using an updated version of the method-of-characteristics computer program described in reference 5. The program was used for defining numerous inlet real-gas, viscid-inviscid flow-field conditions at Mach 5.0, 5.15, 6.0, 6.15, 7.0, 7.15, and 7.25 for various cowl lip positions relative to the inlet spike tip. Analysis results are presented in terms of schedules of mass-flow ratios, aerodynamic contraction ratios, and additive drag, internal-flow shock patterns, and performance parameters including mass-weighted average total-pressure recoveries, throat Mach numbers, and kinetic energy efficiencies.

## SYMBOLS

Values are given in both SI and U.S. Customary Units. The measurements and calculations were made in U.S. Customary Units.

| | |
|---|---|
| $A$ | area, $m^2$ $(ft^2)$ |
| $\frac{A_\infty}{A_{th}}$ | contraction ratio |
| $\frac{A_\infty}{A_{th}}\left(\frac{m}{m_\infty}\right)$ | aerodynamic contraction ratio |
| $C_{D,A}$ | additive drag coefficient |
| $h$ | enthalpy, J/kg (Btu/lb) |
| $h'$ | throat height (inclined $95.645^o$ to the AIM center line) |
| $m/m_\infty$ | ratio of captured mass flow to that free-stream mass flow that passes through an area equal to the projected cowl area $\left(R_C^2 = (22.934 \text{ cm})^2 = (9.029 \text{ in.})^2 = (0.752 \text{ ft})^2\right)$ |
| $M$ | Mach number |
| $p$ | pressure, atm (psia) |
| $q$ | dynamic pressure, atm (psf) |
| $R$ | radius nondimensionalized by $R_{CL}$ (22.86 cm (9.0 in.)) |
| $T$ | temperature, K $(^oR)$ |
| $V$ | velocity, m/sec (ft/sec) |
| $X$ | distance from spike vertex nondimensionalized by $R_{CL}$ (see fig. 1(a)) |
| $y/h'$ | ratio of distance from centerbody surface to throat height |
| $\eta_{KE}$ | inlet kinetic energy efficiency |

$\eta_R$ inlet total-pressure recovery

$\delta$ boundary-layer thickness

$\delta^*$ boundary-layer displacement thickness

Subscripts:

C most forward point on cowl lip (see fig. 1(a))

CL $12^o$ tangent point on cowl lip (see fig. 1(a))

t total

th throat

$\infty$ free stream

1.0 mass-flow ratio of 1.0 (see appendix)

Abbreviation:

*l*ms limiting mesh size

## ANALYSIS

### Analytical Method

The analytical investigation that has been performed for the full-scale inlet of the HRE-AIM used an updated version of the computer program described in reference 5. The program may be exercised for either inviscid or combined viscid-inviscid solutions for real or perfect gas. Results obtained for this investigation were from real-gas, viscid-inviscid computations with laminar boundary-layer transition set to start at an X of 1.89 (corresponds closely to the transition regions of the HRE 2/3-scale inlet tests of ref. 1).

The program incorporates several analytical methods that were listed in reference 5 and are listed herein for convenience:

(1) Method of characteristics

(2) Blunt-body solutions (ref. 6)

(3) Sharp lip viscous interactions (ref. 7)

(4) Laminar boundary layer (ref. 8)

(5) Turbulent boundary layer (ref. 9)

(6) Boundary-layer transition (momentum balance)

(7) Shock—boundary-layer interaction (continuity)

(8) Vortex sheets

(9) Shock wave intersections

Limitations of the computer program indicated in reference 5 are that it is valid for constant wall temperature only (requires some care in wall temperature selection to approximate heat transfer) and it does not compute shocks resulting from wave coalescence. The blunt-body-method solution employed was noted to have convergence problems in that trends for the pressure, density, velocity, and flow inclination yielded by the method are not as smooth as required for input to the method-of-characteristics solutions. However, the blunt-body-method solution is widely accepted and used in supersonic flow near blunt bodies. It was also noted in reference 5 that the computer solutions are sensitive to limiting mesh size ($\ell$ms) as are all method-of-characteristics computer programs. This and other sensitives encountered are discussed in the section "Results and Discussion."

## Analytical Model

The model used in this analytical investigation was the full-scale inlet of the HRE-AIM which is shown schematically in figure 1(a). Coordinates of the inlet are listed in table 1, and the values for the cowl coordinates are for shock-on-lip position at Mach 6.0; other cowl lip locations were analyzed in which the appropriate cowl longitudinal coordinates were used. All X values are measured from the centerbody virtual vertex as shown in the insert sketch of the tip. The $X_C$ values represent the distance from the vertex to the most forward point on the cowl leading edge as shown in the cowl insert. Note in the cowl detail the location of the most forward point $(X_C$ and $R_C)$ on the cowl lip in relation to the $12^o$ tangent point $(X_{CL}$ and $R_{CL})$ generally used in reference 1. Throughout this investigation the $X_C$ and $R_C$ values are used; the $R_C$ value is 22.934 cm (9.029 in.). The inlet throat location indicated in figure 1(a) at X = 4.5 (102.87 cm or 40.5 in.) was used in the present theoretical analysis. Surface measurements of the AIM have recently been reviewed, and the location of the throat station has been more accurately determined to be at 104.78 cm (41.25 in.). Change in the geometric location is not considered significant to the results because of the uncertainties in boundary-layer-thickness predictions and because the region of the throat displacement is one of nearly constant area.

## Analytical Conditions

Experimental tests of the HRE-AIM (photograph shown in fig. 1(b)) are scheduled to be conducted in the Lewis hypersonic tunnel facility (HTF); AIM is shown partially installed in the HTF in the photograph of figure 1(c). Analytical computations were therefore performed in this investigation for the nominal conditions obtainable in the HTF which simulated high and low flight altitudes (see tables 2 and 3 and fig. 2). Calibration Mach numbers shown in table 2 were obtained during facility calibration tests discussed in reference 10. The conditions actually used for the computer computations are listed in table 4. All 23 cases were computed by using the higher total pressures simulating the higher flight dynamic pressure conditions. However, for some Mach 5.0 cases at the higher total pressure, the characteristics solution terminated prior to the throat station; therefore, the cases at the lower total pressures were used as indicated in table 3 (cases 1, 3, and 9).

## Method of Calculation

Computer solutions are generated in two parts by the program. The external flow solution is first computed (generally referred to as job A) and the results in the region of the cowl lip are used to compute the internal flow (referred to as job B). These regions of flow are depicted in the sketch of figure 1(a). When a cowl lip shape and position are included in the input for running job A only, the program will also generate the cowl lip stagnation streamline from which the ratio of the captured free-stream mass flow and the additive drag coefficient are determined.

# RESULTS AND DISCUSSION

The computer program cases listed in table 4 have been analyzed and are discussed in the following paragraphs. The results of these analyses are compared with some results which were presented in reference 1.

## Effect of Cowl Lip Positioning on Internal Flow

Figures 3(a), 3(b), and 3(c) present typical internal flow shock patterns at various cowl lip positions for Mach numbers of 5.0, 6.0, and 7.0, respectively. The bottom sketch of each figure represents the case with the centerbody tip shock nearly impinging upon the cowl lip stagnation point. (For Mach 5.0 (fig. 3(a)) the cowl lip position in the bottom sketch is the same as for the Mach 6 shock-on-lip position.) From the bottom to the top of each page, sketches are arranged in order of increasing distance from the centerbody tip to the cowl lip. As this longitudinal distance increased, both the captured mass flow and the inlet throat area decreased. Also, the flow directed at the blunt cowl lip decreased in Mach number and increased in flow angle relative to the cowl lip internal surface because of greater external compression. This influenced the shape of the cowl lip shock

and the internal shock reflection patterns. These changes in the cowl lip shock shape and the internal shock reflection patterns, of course, affected the inlet performance, including pressure recovery and kinetic energy efficiency. It is interesting to note that for all Mach numbers and cowl positions considered, the cowl lip shock always impinged upon the centerbody in the region of an X of 4.2. This similarity apparently results from a combination of the changes in the shape of the cowl lip shock and the inlet gap height at the cowl lip.

A large region of wave coalescence occurred in the internal flow for all three Mach numbers and for the two most forward positions of the cowl. The computer program does not compute shocks that would result from wave coalescence such as shown in figure 3 but instead employs a computing "bookkeeping" procedure generally accepted for the method of characteristics. The procedure is as follows: as a coalescence of two characteristic rays of the same family occurs, computation of the downstream ray is terminated and the remaining points of the previously computed upstream ray also become the remaining points of the downstream ray. This procedure results in a discontinuity in the field of characteristics in the remaining computations, but without entropy and total-pressure losses that would be present if truly accounting for a new shock. For Mach 5.0 and 6.0 (figs. 3(a) and 3(b), respectively), the large coalescence region exists only at the most forward cowl position (cases 2 and 11) but another region of coalescence occurs prior to the larger region for more rearward cowl positions. Then, as the rearward movement of the cowl continues, the large region is not apparent and only the small region emanating very close to the cowl lip remains. The large region of coalescence was also noted in reference 1 and was stated to be primarily the result of the compression fan originating from the centerbody aft compression surface (see fig. 1(a)) focusing on the cowl inner surface and reflecting from it. The small region of coalescence emanates from the cowl inner surface in the initial compression region along this surface. The absence of these small regions from the Mach 5.0 and 6.0 most forward positions of the cowl lip (cases 2 and 11) and the Mach 7.0 two most forward positions (cases 17 and 18) is not readily explainable.

## Schedules of Mass-Flow Ratio, Additive Drag Coefficient, and Aerodynamic Contraction Ratio

Mass-flow ratio.- The computational results of the cases listed in table 4, along with the results of many job A computer cases, were used to establish the mass-flow-ratio curves presented in figure 4(a) which adequately define the ranges for the AIM tests. The solid lines represent mass flows for the three nominal test Mach numbers, 5, 6, and 7. Short-dash lines represent Mach numbers near the facility nozzle calibrated Mach numbers especially at Mach 5.0 and 7.0 (see table 2). The long-dash line at Mach 4 is from reference 1. Values for the Mach 8 curve of reference 1 could not be obtained

for "spot check" computer cases; therefore, the Mach 8 curve of figure 4(a) was obtained from computations using job A. Values of the Mach 6 curve of figure 4(a) are in agreement with values presented in reference 1. Several cases were run with the centerbody tip shock near the cowl stagnation point to obtain accurate full-capture points (value of 1.0) over the range from Mach 5.0 to Mach 8.0. At the bottom of figure 4(a) are small arrowheads depicting the presently planned cowl lip positions scheduled for testing during the AIM tests.

Table 5 lists the points which define the curves for Mach numbers from 5.0 to 7.25 of figure 4(a). These points were used to construct the curves presented in figure A1 of the appendix (the Mach 8 curve of fig. 4(a) was used to complete the figure up to Mach 8). Points from the curves of figures 4(a) and A1 were "curve fitted" and the mathematical expressions of the curve fits and their limitations are discussed in the appendix. Point values from the curves of figure 4(a) or some similar mathematical expression is to be employed in an AIM data-reduction computer program.

Additive drag coefficients.- Figure 4(b) contains the schedules of additive drag coefficients for Mach 5.0 to 7.25. The schedules correspond to the mass-flow-ratio schedules of figure 4(a). Values of additive drag coefficients which define the curves of figure 4(b) are given in table 6. These results may be used in "checking out" an AIM performance computer program.

Contraction ratios.- The overall geometric-contraction-ratio schedule obtained from reference 1 is represented by the uppermost curve in figure 5. Using this schedule and the mass-flow-ratio values of figure 4(a), aerodynamic-contraction-ratio (geometric contraction ratio multiplied by the captured mass-flow ratio) schedules were obtained and are presented in figure 5. The aerodynamic-contraction-ratio curve for Mach 4 was obtained directly from reference 1. A faired curve through the peak values of the aerodynamic-contraction-ratio schedules is also depicted in figure 5; peak values are used in the discussion of the inlet total-pressure recovery.

## Throat Conditions

Internal flow representation.- Results of the digital computer cases listed in table 4 yielded the conditions for each case at the inlet throat station (X of 4.5). A typical internal flow field produced from the computer results is shown in figure 6 with a tabulation of the conditions at the throat. The numbered points across the throat station are computed points in the characteristic net or are points obtained by straight-line interpolation between two net points. The throat profiles were determined from these point conditions.

Throat profiles.- Throat profiles of local total-pressure ratio $p_t/p_{t,\infty}$ and local Mach number are presented in figures 7 and 8. Figure 7 presents profiles for those cases where the spike tip bow shock is near the cowl lip stagnation point. (Note that at Mach 5.0

and 5.15 the cowl is located near shock-on-lip position at Mach 6.) Profiles for various cowl positions at Mach numbers of 5.0, 6.0, and 7.0 are presented in figures 8(a), 8(b), and 8(c), respectively. The discontinuities in the profiles are caused by the reflected internal shock crossing the throat station; a large discontinuity, however, was not always associated with the crossing of such a shock. Changes in the shapes of these profiles are attributed to the change of the internal shock patterns such as those shown in figure 3. The shapes of the total-pressure-ratio profiles appear to be similar to experimental results of the 2/3-scale inlet investigation reported in reference 1, in that the total pressure is greatest near the centerbody. The lower total pressures next to the cowl are considered to be the result of the cowl lip bluntness affecting the flow next to the cowl surface. The spike tip bluntness effect is very insignificant in the flow next to the centerbody at the throat because the effect on the flow is distributed about a larger area as the flow progresses downstream.

Point values of the throat profiles in figures 7 and 8 represent the inviscid method-of-characteristics solutions. Similar throat condition profiles were generated by using characteristic mesh point conditions obtained from the reference 5 computer results as input to a computer program developed by one of the authors which determined mass-weighted average flow properties at the throat. The portions of the inviscid flow profiles within the boundary layers were replaced by using the boundary-layer-shape exponent values obtained from the reference 5 computer results and assuming a constant static pressure across the boundary layer equal to the pressure at the boundary-layer edge. (Superimposed in fig. 7 are values of the centerbody and cowl boundary-layer edge and displacement thicknesses for Mach 6.0 (case 11).) As a comparison, a total-pressure-ratio profile with the proper boundary-layer conditions is shown for Mach 6.0 full-scale theory from reference 1. Results of the mass-weighted averaging program included the total enthalpy losses and inlet performance parameters.

## Inlet Performance

Total-pressure recovery.- Mass-weighted average total-pressure recoveries are presented in figure 9. Recoveries as a function of free-stream Mach number are shown in figure 9(a) and represent the results when the spike tip shock is nearly impinging on the cowl lip stagnation point. (Note that at Mach 5.0 the cowl is at the position for shock on lip at Mach 6.0.) The short-dash line in figure 9(a) represents theoretical mass-weighted results for the 2/3-scale inlet T-model from reference 1 and the square symbols represent the corresponding mass-weighted 2/3-scale experimental data, also from reference 1. The theoretical mass-weighted results from reference 1 for the full-scale inlet T-model are presented in figure 9(a) and do not exhibit good agreement with the 2/3-scale theoretical trend. (All the theoretical results were obtained by using the updated version of the ref. 5 computer program.) Direct comparison of the present AIM

theoretical results with the results from reference 1 (full-scale theory and the 2/3-scale theory and experimental data) can be made only for Mach 6.0; the agreement is best between the present AIM theory and the full-scale theory and is shown to be within 2 percent. The cowl positions of the present and the reference 1 Mach 6 full-scale cases are slightly different, which may contribute toward the difference of the recovery values.

Pressure recoveries as a function of cowl position are presented in figure 9(b). The arrowheads represent the cowl positions planned for the AIM tests (also depicted in fig. 4(a)). Results for Mach 5.0 indicate a trend as represented by the solid line. The trend curve possesses slightly increasing pressure recovery values with increasing $X_C$ values. The two largest values of cowl position have pressure recovery values that decrease slightly. These two cowl positions are on the decreasing portion of the aerodynamic-contraction-ratio curve (see fig. 5); therefore, the trend curve is shown to start decreasing at the $X_C$ value corresponding to the peak aerodynamic contraction ratio. The trend of slightly increasing recovery values is also representative of two of the Mach 6.0 values (at $X_C$ values of about 3.9 and 4.07). At the point of the peak aerodynamic contraction ratio for Mach 6.0 the decreasing trend is begun and it very nearly represents the last two cowl positions. A Mach 6.0 recovery value was obtained at an $X_C$ of 4.0 which was low with respect to the trend. Computer results for this case indicated thick boundary layers internally (large ratios of boundary-layer thickness to throat channel height) that were about twice as thick as those for the other Mach 6.0 cases. Whether these thick boundary-layer results were truly valid could not be ascertained. The trend was not representative of the Mach 7.0 results; the results instead possessed a continuously decreasing trend. Recovery values for Mach 7.0, 7.15, and 7.25 at an $X_C$ of about 4.06 are for cases that possessed thick internal boundary layers which may account for these values appearing to be low with respect to the other Mach 7.0 recovery values. Since the trend curves are not representative of all cases, they should be treated with caution.

Mach number.- Throat Mach numbers were obtained from the results of the mass-weighted averaging computer program previously mentioned. Throat Mach numbers as a function of free-stream Mach number are presented in figure 10(a). Points representing the full-scale theory of reference 1 were obtained by averaging values of three characteristic net points near the throat station; this should result in slightly greater values than would be obtainable if enough points were given to account for the boundary-layer flow. The dash line is merely a fairing of the present AIM theoretical results. Note that the throat Mach number is 44 to 50 percent of the corresponding free-stream Mach number.

Throat Mach numbers are shown as a function of the cowl lip position in figure 10(b). The straight-line trends are a family of constant slope $(\Delta M/\Delta X_C \approx -2.3)$. At an $X_C$ of 3.747 for Mach 5.0, the value appears rather low because, as shown in the Mach number

profile (case 1) of figure 8(a), the Mach number drops off rapidly next to the centerbody, unlike the other profiles. The exact reason for this was not determined. The well-defined family of trends for the throat Mach number values are acceptable even though the pressure recovery values have poorly defined trends because the Mach number values are highly insensitive to total pressures and are very sensitive to static pressures.

Kinetic energy efficiency.- Values of kinetic energy efficiency were obtained from the mass-weighted averaging computer program. The efficiencies are presented in figure 11(a) as a function of free-stream Mach number for the cases with the spike tip shock nearly impinging on the cowl lip. (Note again that the Mach 5.0 and 5.15 cases have the cowl positioned for near shock on lip at Mach 6.0.) Efficiency values are shown in figure 11(b) as a function of the cowl position. There is no readily evident trend of the efficiencies in either figure; the numerical average value $\bar{\eta}_{KE}$ for both figures is about 0.93.

The kinetic energy efficiencies were computed for a constant cooled-wall temperature of 500 K (900° R) and resulted in throat total-enthalpy losses; ratios of the throat total enthalpy to the free-stream total enthalpy are listed in table 4. The reference 5 computer program could not be operated for wall temperatures low enough to approximate the predicted wall temperatures of the AIM more closely. Enthalpy losses presently computed are therefore less than the expected losses for the AIM tests and thus the presently computed kinetic energy efficiencies should be greater than the expected AIM test results. At Mach 6.0 the AIM inlet total-enthalpy losses are estimated to be about 9 percent, or a total-enthalpy-ratio value of 0.91.

## Effects of Computer Program Sensitivities

Reference 5 indicated that the computer program employed for these analyses was sensitive to some of the input parameters. The effect of the mesh size and other sensitives noted during these analyses are discussed in the following paragraphs.

Relationship between spike tip shock and cowl lip shock.- Computer difficulties were experienced when the spike tip shock was allowed to impinge near the cowl lip stagnation point. There was no reflection of the spike tip shock because the only possible solution in front of the blunt cowl lip is a normal shock wave. If the spike tip shock wave and the cowl lip shock wave were to combine in a reflection to the centerbody, a strong wave solution could exist. In one instance, for Mach 6.0, a resultant shock was computed that was a strong wave solution; however, a reflection of the shock from the centerbody never occurred. Attempts were also made to purposely allow the spike tip shock to impinge upon the cowl inner surface since such a test is planned for the AIM. These attempts were mostly unsuccessful except for one case where the spike tip shock did reach the

cowl inner surface after crossing the cowl lip shock but only a limited amount of flow-field computations was obtained; according to reference 5 this was, however, a complete solution. Successful complete solutions (internal shock reflections) were not obtained for the spike tip shock impinging near the cowl lip until the cowl location was changed slightly to allow the spike tip shock to impinge outside of the cowl lip stagnation point. (It should be noted in relation to the two foregoing shock problems that during the HRE 2/3-scale inlet model tests reported in ref. 1, the spike tip shock was focused as close as was physically possible to the cowl lip stagnation point with no detrimental efficiency losses. Also, the tip shock was allowed to enter the cowl without unstarting or drastically affecting the inlet operation.)

Characteristic net limiting mesh size.- The limiting mesh size ($\ell$ms) has only slight effects on the accuracy of the results of the method of characteristics (the smaller, the more accurate); however, very often the selection of the correct $\ell$ms value was the determining factor of whether a complete and successful computation case was obtained. The standard $\ell$ms value was 3.048 cm (1.2 in.), but in a few cases a more appropriate $\ell$ms value was required.

A solution of interest was case 12 for Mach 6.0 which was run with three different limiting mesh sizes; the resulting internal flow shock patterns are presented in figure 12. With the largest limiting mesh size (4.572 cm (1.8 in.)) the first internal shock reflection occurred just downstream of the impinging shock. As the $\ell$ms value is decreased, the reflection occurs farther downstream. A limiting mesh size of 1.524 cm (0.6 in.) resulted in the shock reflecting downstream of the throat section. The trend of shifting the shock reflection downstream with decreasing limiting mesh size appears to be the result of the cowl lip shock intersecting the centerbody boundary layer in an increasingly more asymptotic manner; the trend is not definite, however, as it was for case 18 (fig. 3(c)) at Mach 7.0. When limiting mesh size was decreased for this case, the reflection of the shock was shifted upstream. It appears that the mesh size changes the shape of the cowl lip shock in that the mesh size affects the boundary-layer growth along the centerbody and thus affects the flow conditions approaching the cowl lip. However, no definite trend of the effect of the limiting mesh size upon the solutions can be concluded. Along the same lines, the boundary-layer solution is sensitive to the surface contour and to the resulting relative locations of expansions and shock wave reflections which, as discussed, are affected by the limiting mesh size. For cases 17 and 18 at Mach 7.0 (fig. 3(c)), the edge of the boundary layer and the displacement thickness appeared to be distorted. This distortion is thought to be the result of the relative location of the expansions and reflected shock waves. A more appropriate $\ell$ms value may resolve the distortions; however, several different values were attempted.

Even though this computer program has limitations and parts which could be improved, the program as a whole appears to be the best available for such inlet design analyses as are presented here.

## SUMMARY OF RESULTS

A theoretical full-scale inlet investigation has been conducted in support of the technology development of the NASA Hypersonic Research Engine (HRE) Project which is scheduled to be culminated with the experimental investigation using the Aerothermodynamic Integration Model (AIM). The theoretical analysis used a method-of-characteristics computer program for defining the AIM inlet flow conditions (real-gas, viscid-inviscid flow) at various inlet cowl lip positions over the range of AIM free-stream test conditions at Mach numbers from 5.0 to 7.25.

Mass-flow ratios and additive drag coefficients were well defined over the range of AIM test conditions. The mass-flow values and mathematical curve fitting expressions obtained for these values are suitable for employment in the AIM data-reduction program.

Mass-weighted average inlet performance parameters, including total-pressure recovery, throat Mach number, and kinetic energy efficiency, as functions of free-stream Mach number and cowl positions were obtained. The results for these performance parameters can be summarized as follows:

1. The pressure recovery decreases with free-stream Mach number.

2. At a free-stream Mach number of 5.0 the pressure recovery increased linearly for a range of cowl positions.

3. The throat Mach number decreased linearly as a function of cowl position for various free-stream Mach numbers.

4. Kinetic energy efficiency results as functions of both free-stream Mach number and cowl position did not possess any definite trends; however, a numerical average of all kinetic-energy-efficiency values was about 0.93.

Langley Research Center,
National Aeronautics and Space Administration,
Hampton, Va., June 11, 1974.

## APPENDIX

## CURVE-FIT EXPRESSIONS

### Cowl Positions as a Function of Mach Number for Constant Values of Mass-Flow Ratios

Quadratic curve fits for points from the family of curves presented in figure A1 have been obtained by using a small digital computer program. Two "fits" were obtained for each curve; one for the Mach number limit from 5.0 to 6.0 and the other for Mach numbers from 6.0 to 7.25. Table A1 presents computer point value results for each mass-flow-ratio curve. The quadratic expression of the curve fits are shown at the bottom of table A1, just below the tabulation of the proper values for constants A, B, C, D, E, and F. These point values are in reasonably good agreement with the curves of figure A1.

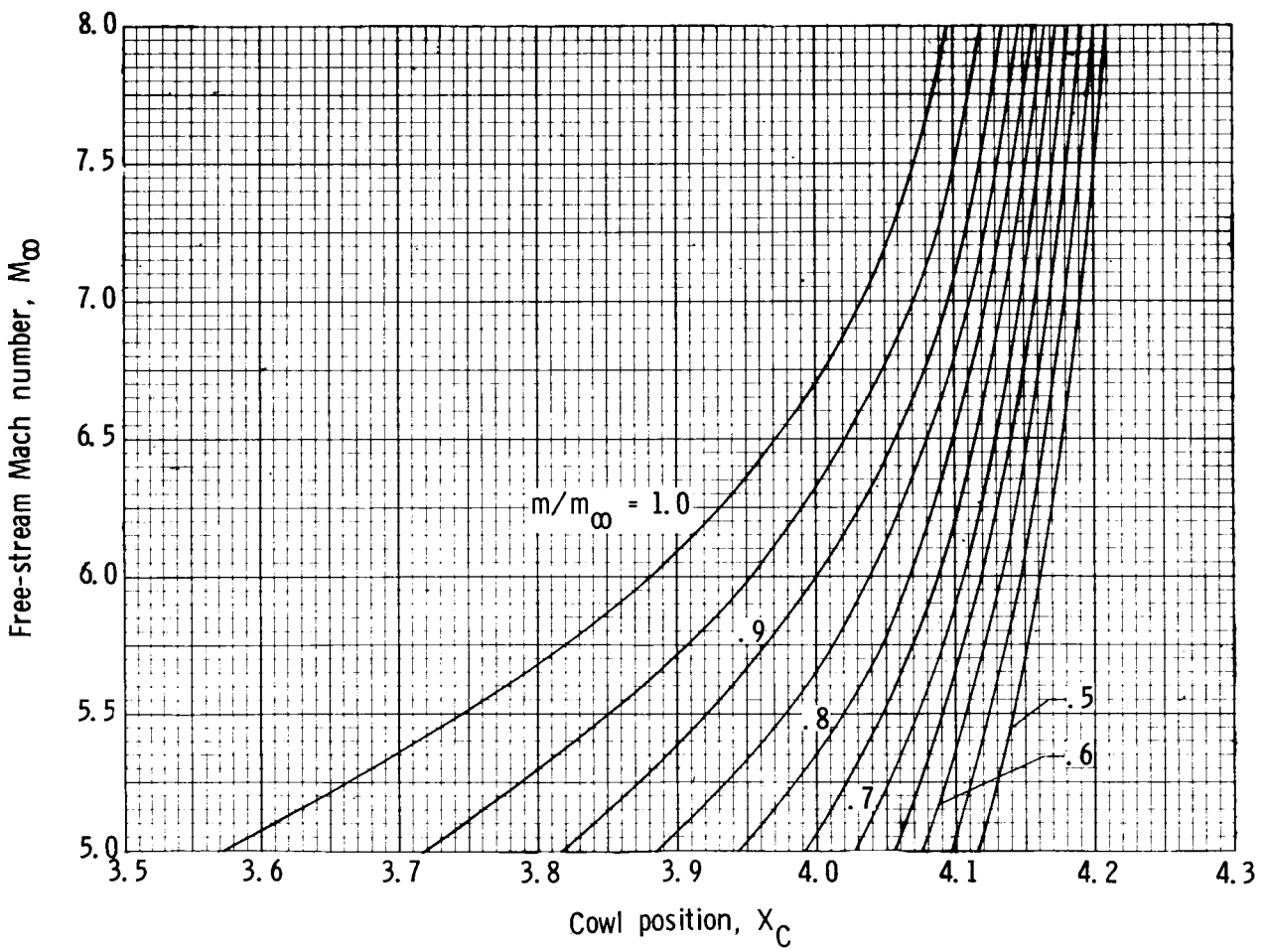


Figure A1.- Effect of free-stream Mach number and cowl position on constant values of mass-flow ratios.

TABLE A1.- COMPUTER POINT VALUE RESULTS FROM QUADRATIC EXPRESSIONS OF CURVES IN FIGURE A1

| $m_\infty$ | $X_C$ at $m/m_\infty$ of – | | | | | | | | | | |
|---|---|---|---|---|---|---|---|---|---|---|---|
| | 1.0 | 0.95 | 0.90 | 0.85 | 0.80 | 0.75 | 0.70 | 0.65 | 0.60 | 0.55 | 0.50 |
| 5.000 | 3.573330 | 3.716800 | 3.817300 | 3.886000 | 3.943300 | 3.991330 | 4.028667 | 4.056000 | 4.076930 | 4.096670 | 4.116000 |
| 5.100 | 3.610985 | 3.746921 | 3.839684 | 3.906907 | 3.960792 | 4.003650 | 4.038361 | 4.063308 | 4.083308 | 4.102097 | 4.121201 |
| 5.200 | 3.647147 | 3.775635 | 3.861213 | 3.926560 | 3.977168 | 4.015410 | 4.047635 | 4.070429 | 4.089538 | 4.107474 | 4.126269 |
| 5.300 | 3.681815 | 3.802941 | 3.881887 | 3.944960 | 3.992428 | 4.026610 | 4.056488 | 4.077363 | 4.095618 | 4.112800 | 4.131203 |
| 5.400 | 3.714989 | 3.828839 | 3.901706 | 3.962107 | 4.006572 | 4.037250 | 4.064919 | 4.084110 | 4.101548 | 4.118075 | 4.136003 |
| 5.500 | 3.746670 | 3.853330 | 3.920670 | 3.978000 | 4.019600 | 4.047330 | 4.072930 | 4.090670 | 4.107330 | 4.123300 | 4.140670 |
| 5.600 | 3.776857 | 3.876413 | 3.938779 | 3.992640 | 4.031512 | 4.056850 | 4.080520 | 4.097043 | 4.112962 | 4.128474 | 4.145203 |
| 5.700 | 3.805550 | 3.898088 | 3.956034 | 4.006027 | 4.042308 | 4.065810 | 4.087689 | 4.103230 | 4.118446 | 4.133598 | 4.149603 |
| 5.800 | 3.832749 | 3.918355 | 3.972433 | 4.018160 | 4.051988 | 4.074210 | 4.094437 | 4.109229 | 4.123780 | 4.138672 | 4.153869 |
| 5.900 | 3.858455 | 3.937215 | 3.987977 | 4.029040 | 4.060552 | 4.082050 | 4.100764 | 4.115041 | 4.128964 | 4.143695 | 4.158001 |
| 6.000 | 3.882667 | 3.954667 | 4.002667 | 4.038667 | 4.068000 | 4.089330 | 4.106670 | 4.120667 | 4.134000 | 4.148667 | 4.162000 |
| 6.125 | 3.907598 | 3.973338 | 4.018046 | 4.050316 | 4.076447 | 4.096461 | 4.112903 | 4.126444 | 4.139009 | 4.153007 | 4.166217 |
| 6.250 | 3.930811 | 3.990807 | 4.032349 | 4.061242 | 4.084469 | 4.103201 | 4.118779 | 4.131885 | 4.143795 | 4.157182 | 4.170261 |
| 6.375 | 3.952306 | 4.007076 | 4.045574 | 4.071447 | 4.092065 | 4.109551 | 4.124298 | 4.136990 | 4.148355 | 4.161193 | 4.174133 |
| 6.500 | 3.972083 | 4.022144 | 4.057723 | 4.080930 | 4.099236 | 4.115510 | 4.129460 | 4.141760 | 4.152692 | 4.165040 | 4.177832 |
| 6.625 | 3.990142 | 4.036011 | 4.068795 | 4.089691 | 4.105982 | 4.121079 | 4.134265 | 4.146194 | 4.156804 | 4.168722 | 4.181358 |
| 6.750 | 4.006483 | 4.048677 | 4.078790 | 4.097730 | 4.112302 | 4.126257 | 4.138713 | 4.150293 | 4.160692 | 4.172240 | 4.184712 |
| 6.875 | 4.021106 | 4.060141 | 4.087708 | 4.105047 | 4.118197 | 4.131045 | 4.142803 | 4.154055 | 4.164355 | 4.175593 | 4.187893 |
| 7.000 | 4.034011 | 4.070405 | 4.095549 | 4.111642 | 4.123667 | 4.135443 | 4.146537 | 4.157483 | 4.167795 | 4.178782 | 4.190901 |
| 7.125 | 4.045198 | 4.079468 | 4.102313 | 4.117516 | 4.128711 | 4.139450 | 4.149913 | 4.160574 | 4.171009 | 4.181807 | 4.193737 |
| 7.250 | 4.054667 | 4.087330 | 4.108000 | 4.122667 | 4.133330 | 4.143067 | 4.152933 | 4.163330 | 4.174000 | 4.184667 | 4.196400 |
| A | -0.213935 | 0.415885 | 1.608085 | 1.242685 | 1.645800 | 2.661330 | 3.007272 | 3.452285 | 3.567780 | 3.760905 | 3.685600 |
| B | 1.130883 | 1.012113 | .655573 | .841993 | .738500 | .406000 | .309509 | .167473 | .139130 | .079783 | .119480 |
| C | -.074686 | -.070386 | -.042746 | -.062666 | -.055800 | -.028000 | -.021046 | -.009346 | -.007460 | -.002526 | -.006680 |
| D | .665611 | 1.646116 | 1.998024 | 2.630559 | 3.162352 | 3.287897 | 3.387571 | 3.448660 | 3.629728 | 3.746999 | 3.756528 |
| E | .866032 | 0.615347 | .540872 | .373293 | .232605 | .208537 | .188407 | .176446 | .127117 | .098513 | .100731 |
| F | -.054976 | -.038431 | -.034461 | -.023101 | -.013611 | -.012494 | -.011426 | -.010741 | -.007179 | -.005261 | -.005525 |

$X_C = A + BM + CM^2 \qquad (5.0 \geq M \geq 6.0)$

$X_C = D + EM + FM^2 \qquad (6.0 \geq M \geq 7.25)$

## APPENDIX

### Mass-Flow Ratios as Functions of Mach Number and Cowl Position

An exponential curve fit was obtained of points defining the mass-flow ratios; the mass-flow ratios were approximated reasonably well with certain limitations. The expression for the curve fit was obtained by using the difference between the curve for a mass-flow ratio of 1.0 and the other curves of figure A1. The difference $1.0 - \frac{m}{m_\infty}$ was plotted in figure A2 as a function of a cowl position parameter $\frac{X_C - X_{C,1.0}}{X_{C,1.0}}$ for the

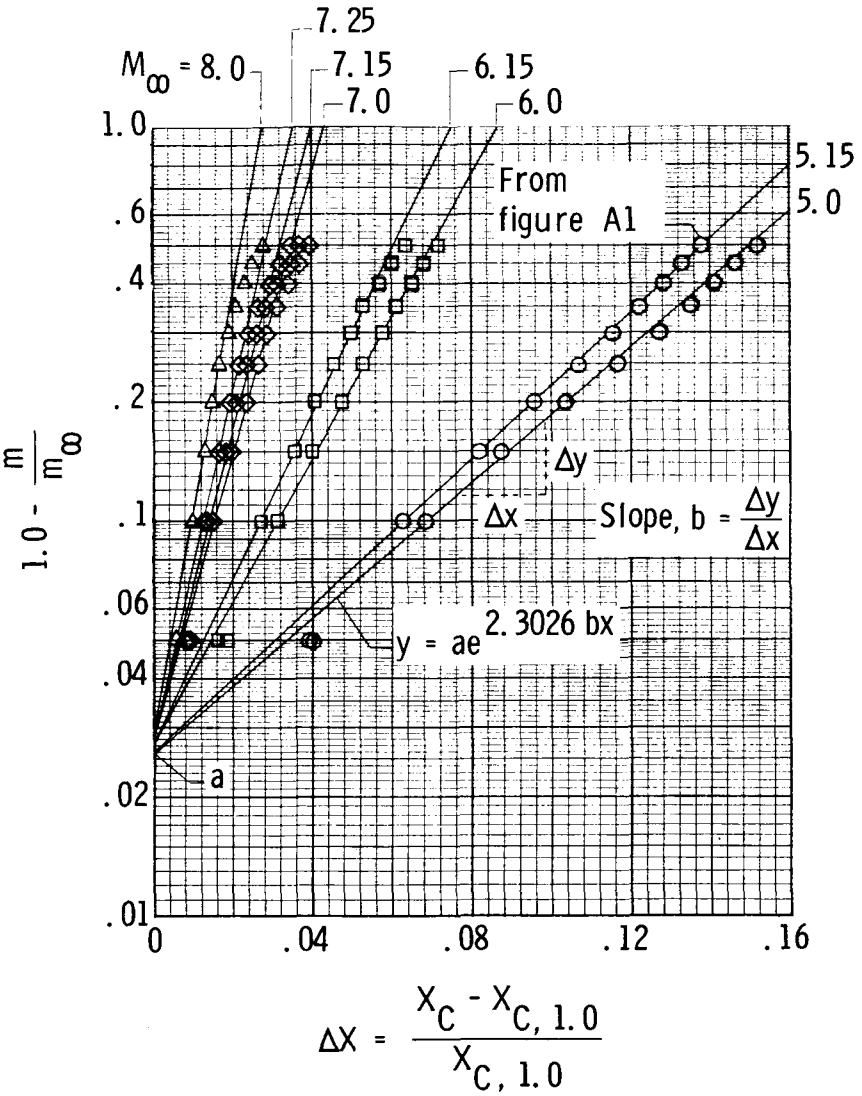


Figure A2.- Mass-flow parameter.

various free-stream Mach numbers. The values for each Mach number are connected with a straight-line fairing which reasonably well represents the point values in the range of $1.0 - \frac{m}{m_\infty}$ from 0.1 to 0.3. The expression for such curves is

## APPENDIX

$$y = ae^{2.3026bx} \tag{A1}$$

where, for the present curves,

$$y = 1.0 - \frac{m}{m_\infty}$$

$$x = \Delta x = \frac{X_C - X_{C,1.0}}{X_{C,1.0}}$$

a represents the y-intercept, and b is the slope expressed as

$$b = \frac{\Delta y}{\Delta x} = \frac{\Delta\left(1.0 - \frac{m}{m_\infty}\right)}{\Delta\left(\frac{X_C - X_{C,1.0}}{X_{C,1.0}}\right)}$$

For $5.0 \leqq M \leqq 6.0$

$$X_{C,1.0} = -0.213935 + 1.130883M - 0.074686M^2$$

and for $6.0 \leqq M \leqq 7.25$

$$X_{C,1.0} = 0.665611 + 0.866032M - 0.054976M^2$$

A plot of the y-intercepts as a function of free-stream Mach number is somewhat random and is therefore represented by a straight line in figure A3; the equation for this

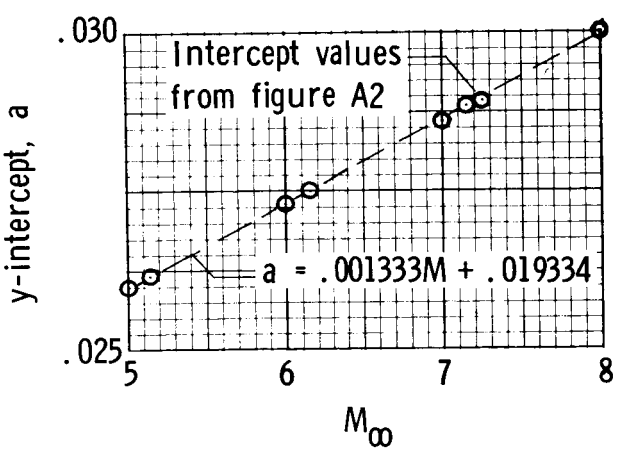


Figure A3.- y-intercepts of the mass-flow parameters.

straight line defines the y-intercepts for the various Mach numbers as

$$a = 0.001333M + 0.019334$$

Values of the slopes determined from figure A2 were plotted in figure A4 as a function of Mach number.

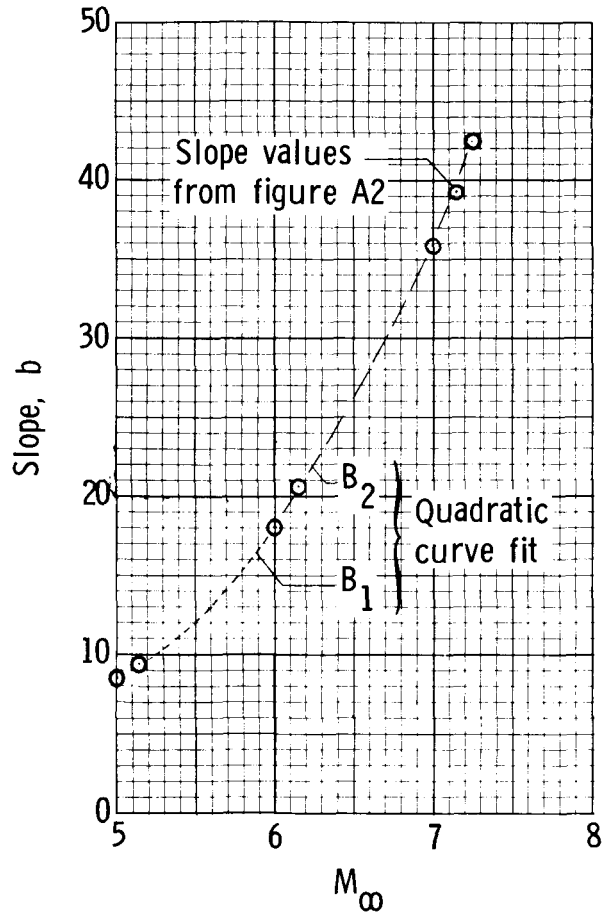


Figure A4.- Slopes of the mass-flow parameters.

A quadratic expression was obtained for the curve from Mach 5.0 to 6.0 and another was obtained for the curve from Mach 6.0 to 7.25. The expression for $5.0 \leqq M \leqq 6.0$ is

$$b = B_1 = 126.30424 - 51.12572M + 5.51528M^2$$

and for $6.0 \leqq M \leqq 7.25$ is

$$b = B_2 = 105.899902 - 42.936332M + 4.717169M^2$$

Therefore, by substituting the expressions just discussed into equation (A1), the mass-flow ratio is defined as

$$\frac{m}{m_\infty} = 1.0 - ae^{2.3026bx} \tag{A2}$$

Equation (A2) was used in developing a small digital computer program which produced results that agreed with the curves of figure A2, that is, matched the point values as closely as the straight line matched the values. The mass-flow ratio was forced to a limiting value of 1.0.

## REFERENCES


1. Pearson, L. W.: Hypersonic Research Engine Project. Phase IIA – Inlet Program. Final Technical Data Report. AP-69-4883 (Contract NAS 1-6666), AiResearch Manufacturing Co., Mar. 27, 1969. (Available as NASA CR-66797.)

2. Engineering Staff: Hypersonic Research Engine Project. Phase II – Combustor Program. Final Technical Data Report. Doc. No. AP-70-6054 (Contract No. NAS 1-6666), AiResearch Manufacturing Co., Mar. 23, 1970. (Available as NASA CR-66932.)

3. Engineering Staff: Hypersonic Research Engine Project. Phase IIA – Nozzle Program. Terminal Summary Report. AP-68-4451 (Contract No. NAS 1-6666), AiResearch Manufacturing Co., Dec. 17, 1968. (Available as NASA CR-101532.)

4. Kay, Ira W.; and McVey, John B.: Hydrocarbon-Fueled Scramjet. Vol. X – Wall Divergence Investigation. AFAPL-TR-68-146, Vol. X, U.S. Air Force, Dec. 1971.

5. Maslowe, S. A.; and Benson, J. L.: Computer Program for the Design and Analysis of Hypersonic Inlets. Report No. 18079 (Contract NAS 2-1460), Lockheed-California Co., Aug. 10, 1964. (Available as NASA CR-77749.)

6. Lomax, Harvard; and Inouye, Mamoru: Numerical Analysis of Flow Properties About Blunt Bodies Moving at Supersonic Speeds in an Equilibrium Gas. NASA TR R-204, July 1964.

7. Hayes, Wallace, D.; and Probstein, Ronald F.: Hypersonic Flow Theory. Academic Press, Inc., 1959.

8. Cohen, Nathaniel B.: Boundary-Layer Similar Solutions and Correlation Equations for Laminar Heat-Transfer Distribution in Equilibrium Air at Velocities up to 41,000 Feet Per Second. NASA TR R-118, 1961.

9. Miller, Leonard D.: Predicting Turbulent Compressible Boundary Layers in Strong Adverse Pressure Gradients. J. Spacecraft & Rockets, vol. 5, no. 8, Aug. 1968, pp. 959-963.

10. Cullom, Richard R.; and Lezberg, Erwin A.: Calibration of Lewis Hypersonic Tunnel Facility at Mach 5, 6, and 7. NASA TN D-7100, 1972.

TABLE 1.- HRE-AIM INLET COORDINATES USED IN THE PRESENT AIM THEORETICAL ANALYSIS

[Mach 6.0 cowl design position]

(a) Spike

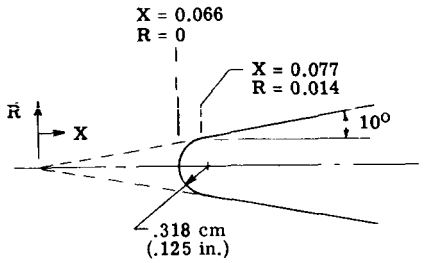


| X | R | |
|---|---|---|
| 0.066 | 0.0 | |
| .077 | .014 | Straight Line |
| 2.040 | .360 | 10.0° |
| 2.145 | .379 | |
| 2.271 | .404 | |
| 2.410 | .432 | |
| 2.537 | .458 | |
| 2.650 | .482 | |
| 2.875 | .531 | |
| 2.974 | .554 | |
| 3.100 | .584 | |
| 3.212 | .613 | |
| 3.295 | .636 | Straight Line |
| 3.373 | .658 | 15.819° |
| 3.640 | .740 | |
| 3.787 | .793 | Straight Line |
| 4.190 | .956 | 22.0° |
| 4.230 | .971 | |
| 4.274 | .984 | |
| 4.308 | .991 | |
| 4.341 | .997 | |
| 4.374 | 1.003 | |
| 4.408 | 1.087 | |
| 4.411 | 1.013 | |
| 4.500 | 1.020 | Throat |
| 4.602 | 1.030 | |
| 4.659 | 1.035 | |
| 4.714 | 1.040 | |

(b) Cowl

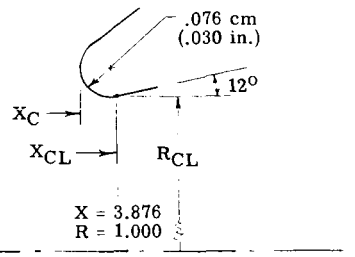


| X | R | |
|---|---|---|
| 3.876 | 1.0 | 12° |
| 3.933 | 1.012 | |
| 3.986 | 1.021 | 10° |
| 4.019 | 1.027 | |
| 4.046 | 1.031 | 8° |
| 4.085 | 1.036 | |
| 4.166 | 1.044 | Straight Line |
| 5.326 | 1.159 | 5.645° |

TABLE 2.- EXPERIMENTAL FREE-STREAM CONDITIONS

| Nominal Mach number | $p_{t,\infty}$ | | $T_{t,\infty}$ | | Simulated altitude (a) | | Calibrated Mach number (b) |
|---|---|---|---|---|---|---|---|
| | atm | psia | K | $^{o}R$ | km | ft | |
| 5.0 | 14.08 | 207 | 1248 | 2245 | 25.30 | 83 000 | 5.18 |
| 5.0 | 28.57 | 420 | 1225 | 2204 | 20.71 | 68 000 | 5.18 |
| 6.0 | 31.70 | 466 | 1665 | 2995 | 27.72 | 91 000 | 6.05 |
| 6.0 | 63.22 | 930 | 1628 | 2930 | 23.16 | 76 000 | 6.05 |
| 7.0 | [c]34.00 | [c]500 | 2211 | 3980 | 34.59 | 113 500 | 7.25 |
| 7.0 | [d]68.00 | [d]1000 | 2130 | 3835 | 29.87 | 98 000 | 7.25 |

[a]For nominal Mach numbers and free-stream static pressures.

[b]From reference 10.

[c]Arbitrarily selected as half of AIM design pressure.

[d]Maximum AIM design operating pressure.

TABLE 3.- HRE FLIGHT ENVIRONMENT

| Mach number | Altitude | | Static pressure, $p_{\infty}$ | | Static temperature, $T_{\infty}$ | | Total pressure, $p_{t,\infty}$ | | Total temperature, $T_{t,\infty}$ | | Dynamic pressure, $q_{\infty}$ | |
|---|---|---|---|---|---|---|---|---|---|---|---|---|
| | km | ft | atm | psia | K | $^{o}R$ | atm | psia | K | $^{o}R$ | atm | psfa |
| 5.0 | 20.11 | 66 000 | 0.0536 | 0.788 | 216.8 | 390.1 | 30.95 | 455 | 1222 | 2200 | 0.937 | 1983 |
| | 20.71 | 68 000 | .0481 | .707 | 217.3 | 391.2 | 28.23 | 415 | 1225 | 2204 | .852 | 1802 |
| | 25.3 | 83 000 | .02401 | .353 | 222.0 | 399.3 | 14.08 | 207 | 1248 | 2245 | .420 | 889 |
| 6.0 | 22.24 | 73 000 | .03842 | .565 | 218.9 | 393.9 | 72.75 | 1070 | 1628 | 2930 | .964 | 2041 |
| | 23.16 | 76 000 | .03333 | .490 | 219.8 | 395.5 | 63.22 | 930 | 1628 | 2930 | .840 | 1777 |
| | 27.72 | 91 000 | .0166 | .244 | 224.2 | 403.7 | 31.70 | 466 | 1665 | 2995 | .4175 | 884 |
| 7.0 | 24.38 | 80 000 | .02769 | .407 | 221.0 | 397.7 | 154.5 | 2270 | 2089 | 3760 | .9475 | 2005 |
| | 25.17 | 82 600 | .0245 | .360 | 221.8 | 399.1 | 137.5 | 2020 | 2095 | 3770 | .840 | 1776 |
| | 29.72 | 97 600 | .01259 | .185 | 225.0 | 406.9 | 70.0 | 1030 | 2129 | 3830 | .4322 | 915 |

TABLE 4.- CONDITIONS FOR AND RESULTS FROM THE THEORETICAL COMPUTER PROGRAM CASES

[$T_{wall}$ = 500 K (900° R)]

| Case | $M_\infty$ | $X_C$ | $m/m_\infty$ | $C_{D,A}$ | $\frac{h_{t,th}}{h_{t,\infty}}$ | $\delta_{th}/h'$ | | $\delta^*_{th}/h'$ | | $p_{t,\infty}$ | | $T_{t,\infty}$ | | $\frac{p_{th}}{p_\infty}$ (a) | $M_{th}$ mass weighted | $\eta_R$ mass weighted | $\eta_{KE}$ mass weighted |
|---|---|---|---|---|---|---|---|---|---|---|---|---|---|---|---|---|---|
| | | | | | | Centerbody | Cowl | Centerbody | Cowl | atm | psia | K | °R | | | | |
| 1 | 5.0 | 3.7467 | 0.9350 | 0.00392 | 0.97486 | 0.26272 | 0.13177 | 0.06557 | 0.02775 | 14.08 | 207 | 1248 | 2245 | 16.792 | 2.596 | 0.5980 | 0.9206 |
| 2 | ↓ | 3.8760 | .8589 | .01117 | .97709 | .25189 | .13732 | .05748 | .02953 | 28.57 | 420 | 1225 | 2204 | 17.958 | 2.599 | .6228 | .9308 |
| 3 | | 3.9627 | .7776 | .02135 | .97342 | .23365 | .15807 | .05399 | .03954 | 14.08 | 207 | 1248 | 2245 | 19.694 | 2.590 | .6536 | .9321 |
| 4 | | 3.9960 | .7442 | .02657 | .97879 | .25896 | .09943 | .05983 | .01835 | 28.57 | 420 | 1225 | 2204 | 23.481 | 2.411 | .6296 | .9326 |
| 5 | | 4.0357 | .6864 | .03678 | .97876 | .19660 | .10023 | .04178 | .01576 | ↓ | ↓ | ↓ | ↓ | 32.184 | 2.259 | .6365 | .9392 |
| 6 | | 4.0660 | .6295 | .04915 | .97629 | .21555 | .09469 | .04530 | .01648 | | | | | 32.132 | 2.225 | .6348 | .9340 |
| 7 | | 4.1013 | .5394 | .07331 | .97477 | .23360 | .09805 | .04975 | .01766 | | | | | 28.987 | 2.285 | .5925 | .9301 |
| [b]8 | | 4.1303 | .4639 | .09358 | | | | | | | | | | | | | |
| 9 | 5.15 | 3.9200 | .8454 | .01304 | .97690 | .22656 | .15905 | .05444 | .03435 | 14.08 | 207 | 1248 | 2245 | 23.741 | 2.554 | .6180 | .9360 |
| 10 | 5.15 | 3.9627 | .8091 | .01777 | .97748 | .24516 | .11664 | .05482 | .02134 | 28.57 | 420 | 1225 | 2204 | 25.835 | 2.472 | .6160 | .9352 |
| 11 | 6.0 | 3.9067 | .9856 | .00131 | .97412 | .22184 | .13379 | .05310 | .02699 | 63.22 | 930 | 1628 | 2930 | 27.060 | 2.976 | .5875 | .9345 |
| 12 | ↓ | 3.9960 | .9088 | .00917 | .96981 | .35420 | .12553 | .10311 | .02248 | ↓ | ↓ | ↓ | ↓ | 28.718 | 2.888 | .4800 | .9321 |
| 13 | | 4.0660 | .8032 | .02498 | .97644 | .21059 | .06423 | .05079 | .01064 | | | | | 42.148 | 2.777 | .6146 | .9454 |
| 14 | | 4.1013 | .7197 | .04272 | .97392 | .21732 | .10100 | .04997 | .01587 | | | | | 41.572 | 2.632 | .5510 | .9296 |
| 15 | | 4.1200 | .6652 | .05689 | .97286 | .23205 | .11201 | .05638 | .01744 | | | | | 38.213 | 2.654 | .4621 | .9243 |
| [b]16 | 6.15 | 3.9160 | .9997 | .00001 | | | | | | | | | | | | | |
| 17 | 7.0 | 4.0360 | .9966 | .00046 | .97052 | .19452 | .12647 | .05063 | .02063 | 68.00 | 1000 | 2130 | 3835 | 55.994 | 3.156 | .5136 | .9401 |
| 18 | ↓ | 4.0593 | .9655 | .00448 | .97186 | .37289 | .12813 | .11429 | .02506 | ↓ | ↓ | ↓ | ↓ | 41.157 | 3.195 | .3952 | .9280 |
| 19 | | 4.0860 | .9169 | .01230 | .96912 | .28504 | .10406 | .07845 | .01734 | | | | | 62.314 | 2.980 | .4656 | .9326 |
| 20 | | 4.1260 | .8030 | .03657 | .97091 | .23793 | .13567 | .06047 | .02470 | | | | | 61.044 | 2.986 | .4354 | .9331 |
| 21 | | 4.1600 | .6300 | .08213 | .97136 | .51256 | .28048 | .12570 | .04448 | | | | | 60.565 | 2.891 | .3647 | .9268 |
| 22 | 7.15 | 4.0627 | .9980 | .00022 | .96192 | .45731 | .10891 | .13646 | .01923 | | | | | 49.474 | 3.154 | .3958 | .9156 |
| 23 | 7.25 | 4.0580 | .9980 | .00013 | .97284 | .34710 | .11998 | .10889 | .02441 | ↓ | ↓ | ↓ | ↓ | 46.374 | 3.261 | .4060 | .9304 |

[a]Values correspond to mass-weighted Mach numbers.

[b]Incomplete throat flow conditions.

TABLE 5.- VALUES DEFINING THE CURVES[a] OF MASS-FLOW RATIOS AS A FUNCTION OF COWL POSITION FOR CONSTANT MACH NUMBERS

| $m/m_\infty$ | Cowl lip position $X_C$ at $M_\infty$ of – | | | | | | |
|---|---|---|---|---|---|---|---|
| | 5.0 | 5.15 | 6.0 | 6.15 | 7.0 | 7.15 | 7.25 |
| 1.00 | 3.5733 | 3.6227 | 3.8827 | 3.9165 | 4.0307 | 4.0453 | 4.0547 |
| .95 | 3.7168 | 3.7633 | 3.9547 | 3.9813 | 4.0680 | 4.0800 | 4.0873 |
| .90 | 3.8173 | 3.8500 | 4.0027 | 4.0235 | 4.0927 | 4.1027 | 4.1080 |
| .85 | 3.8860 | 3.9187 | 4.0387 | 4.0560 | 4.1107 | 4.1173 | 4.1227 |
| .80 | 3.9433 | 3.9701 | 4.0680 | 4.0773 | 4.1253 | 4.1293 | 4.1333 |
| .75 | 3.9913 | 4.0100 | 4.0893 | 4.0960 | 4.1360 | 4.1400 | 4.1431 |
| .70 | 4.0287 | 4.0407 | 4.1067 | 4.1113 | 4.1463 | 4.1500 | 4.1529 |
| .65 | 4.0560 | 4.0653 | 4.1207 | 4.1253 | 4.1567 | 4.1607 | 4.1633 |
| .60 | 4.0769 | 4.0867 | 4.1340 | 4.1400 | 4.1667 | 4.1707 | 4.1740 |
| .55 | 4.0967 | 4.1047 | 4.1487 | 4.1533 | 4.1780 | 4.1827 | 4.1847 |
| .50 | 4.1160 | 4.1233 | 4.1620 | 4.1667 | 4.1900 | 4.1940 | 4.1964 |
| .45 | 4.1333 | 4.1420 | 4.1767 | 4.1807 | 4.2027 | 4.2060 | 4.2087 |
| .40 | 4.1520 | 4.1600 | 4.1907 | 4.1953 | 4.2153 | 4.2187 | 4.2213 |
| .35 | 4.1713 | 4.1780 | 4.2067 | 4.2100 | 4.2293 | 4.2320 | 4.2340 |
| .30 | 4.1907 | 4.1973 | 4.2227 | 4.2260 | 4.2427 | 4.2460 | 4.2473 |
| .25 | 4.2127 | 4.2173 | 4.2400 | 4.2431 | 4.2571 | 4.2600 | 4.2620 |
| .20 | 4.2380 | 4.2387 | 4.2573 | 4.2607 | 4.2727 | 4.2753 | 4.2760 |
| .15 | 4.2593 | 4.2627 | 4.2773 | 4.2793 | 4.2887 | 4.2901 | 4.2913 |
| .10 | 4.2847 | 4.2880 | 4.2980 | 4.2993 | 4.3053 | 4.3073 | 4.3080 |
| .05 | 4.3127 | 4.3007 | 4.3196 | 4.3200 | 4.3237 | 4.3239 | 4.3240 |
| .0 | 4.3433 | 4.3433 | 4.3433 | 4.3433 | 4.3433 | 4.3433 | 4.3433 |

[a]See figures 4(a) and A1.

TABLE 6.- VALUES DEFINING THE CURVES[a] OF ADDITIVE DRAG COEFFICIENTS AS A FUNCTION OF COWL POSITION FOR CONSTANT MACH NUMBERS

| $C_{D,A}$ | Cowl lip position $X_C$ at $M_\infty$ of – | | | | | | |
|---|---|---|---|---|---|---|---|
| | 5.0 | 5.15 | 6.0 | 6.15 | 7.0 | 7.15 | 7.25 |
| 0.000 | 3.5733 | 3.6227 | 3.8827 | 3.9165 | 4.0307 | 4.0453 | 4.0547 |
| .005 | 3.7780 | 3.8070 | 3.9535 | 3.9735 | 4.0615 | 4.0695 | 4.0755 |
| .010 | 3.8610 | 3.8860 | 3.9975 | 4.0115 | 4.0820 | 4.0880 | 4.0910 |
| .015 | 3.9120 | 3.9340 | 4.0280 | 4.0390 | 4.0965 | 4.1005 | 4.1045 |
| .020 | 3.9530 | 3.9720 | 4.0505 | 4.0590 | 4.1075 | 4.1115 | 4.1125 |
| .025 | 3.9835 | 4.0010 | 4.0670 | 4.0735 | 4.1150 | 4.1185 | 4.1205 |
| .030 | 4.0095 | 4.0240 | 4.0800 | 4.0830 | 4.1200 | 4.1230 | 4.1250 |
| .035 | 4.0300 | 4.0415 | 4.0895 | 4.0925 | 4.1235 | 4.1275 | 4.1295 |
| .040 | 4.0450 | 4.0555 | 4.0965 | 4.1000 | 4.1280 | 4.1305 | 4.1330 |
| .045 | 4.0575 | 4.0645 | 4.1030 | 4.1080 | 4.1315 | 4.1335 | 4.1360 |
| .050 | 4.0660 | 4.0725 | 4.1110 | 4.1145 | 4.1350 | 4.1380 | 4.1400 |
| .055 | 4.0730 | 4.0800 | 4.1180 | 4.1210 | 4.1390 | 4.1415 | 4.1435 |
| .060 | 4.0815 | 4.0875 | 4.1240 | 4.1275 | 4.1425 | 4.1455 | 4.1475 |
| .065 | 4.0900 | 4.0950 | 4.1300 | 4.1330 | 4.1465 | 4.1495 | 4.1510 |
| .070 | 4.0970 | 4.1015 | 4.1350 | 4.1385 | 4.1500 | 4.1530 | 4.1550 |
| .075 | 4.1035 | 4.1090 | 4.1400 | 4.1430 | 4.1540 | 4.1570 | 4.1590 |
| .080 | 4.1100 | 4.1166 | 4.1445 | 4.1480 | 4.1580 | 4.1505 | 4.1525 |
| .085 | 4.1185 | 4.1230 | 4.1500 | 4.1525 | 4.1615 | 4.1650 | 4.1665 |
| .090 | 4.1255 | 4.1300 | 4.1540 | 4.1575 | 4.1650 | 4.1680 | 4.1695 |
| .095 | 4.1325 | 4.1370 | 4.1595 | 4.1620 | 4.1690 | 4.1720 | 4.1735 |
| .100 | 4.1395 | 4.1425 | 4.1625 | 4.1655 | 4.1730 | 4.1755 | 4.1780 |

[a]See figure 4(b).

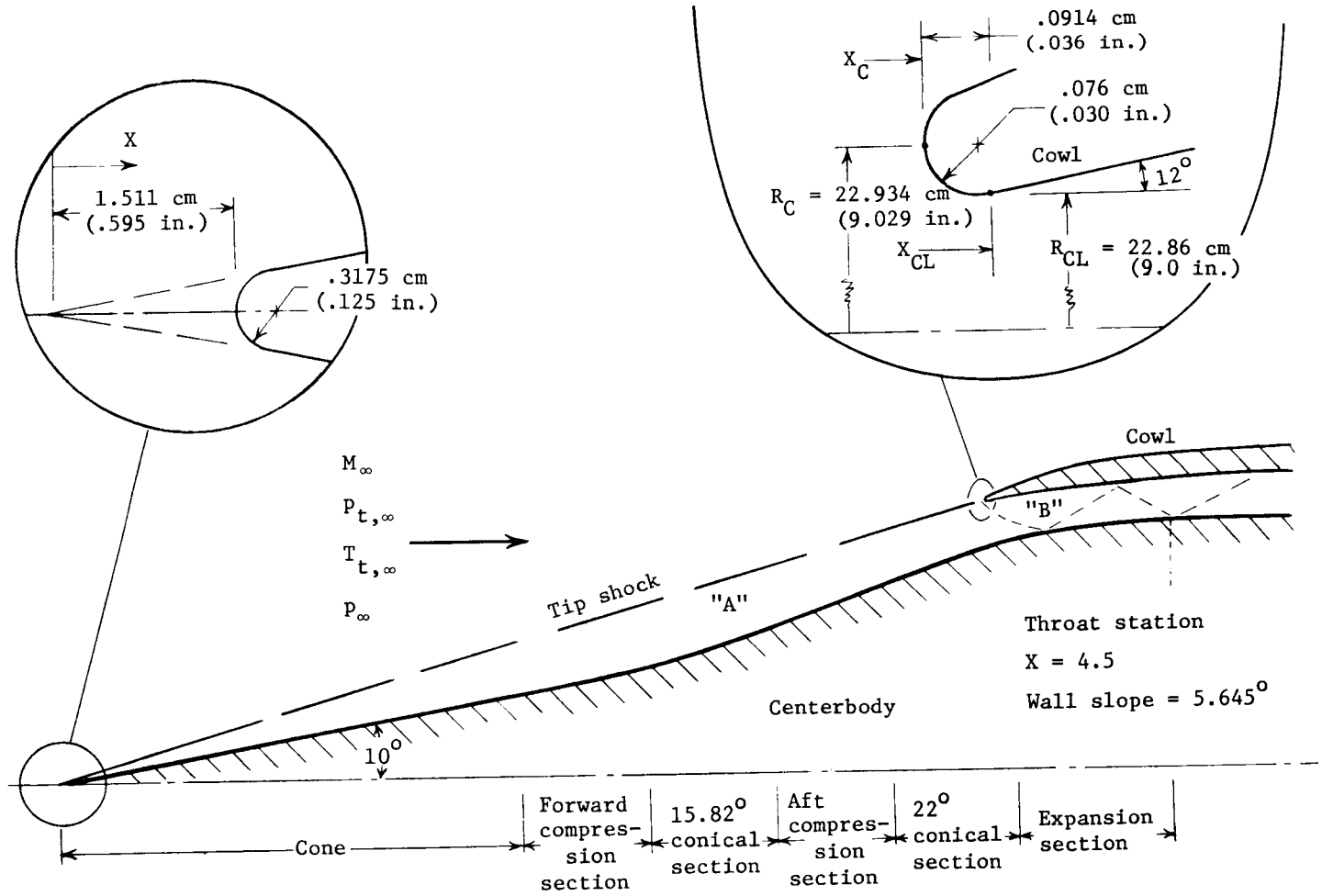


(a) AIM schematic.

Figure 1.- Hypersonic Research Engine (HRE) Aerothermodynamic Integration Model (AIM).

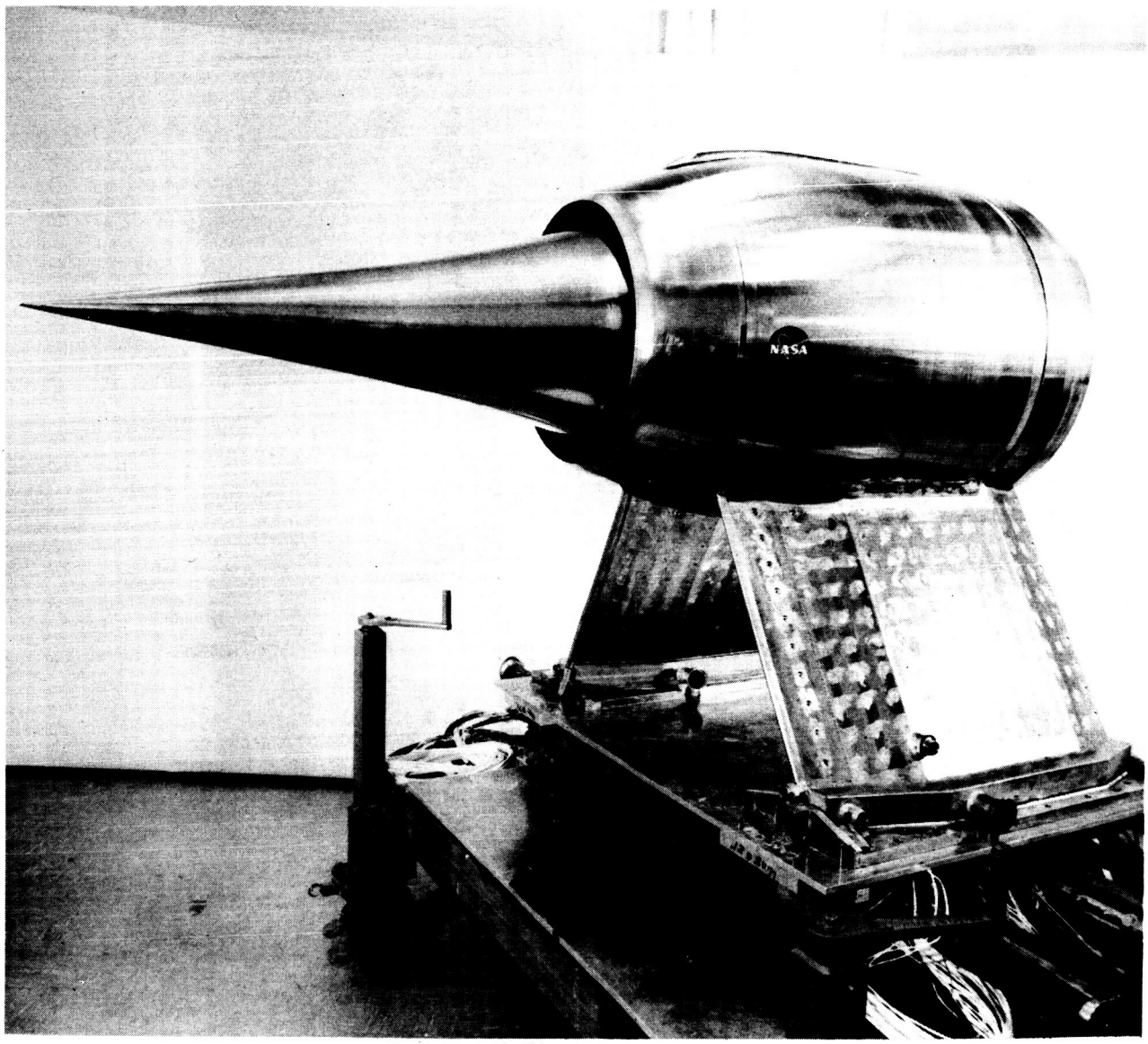


(b) Pretest photograph of AIM.

Figure 1.- Continued.

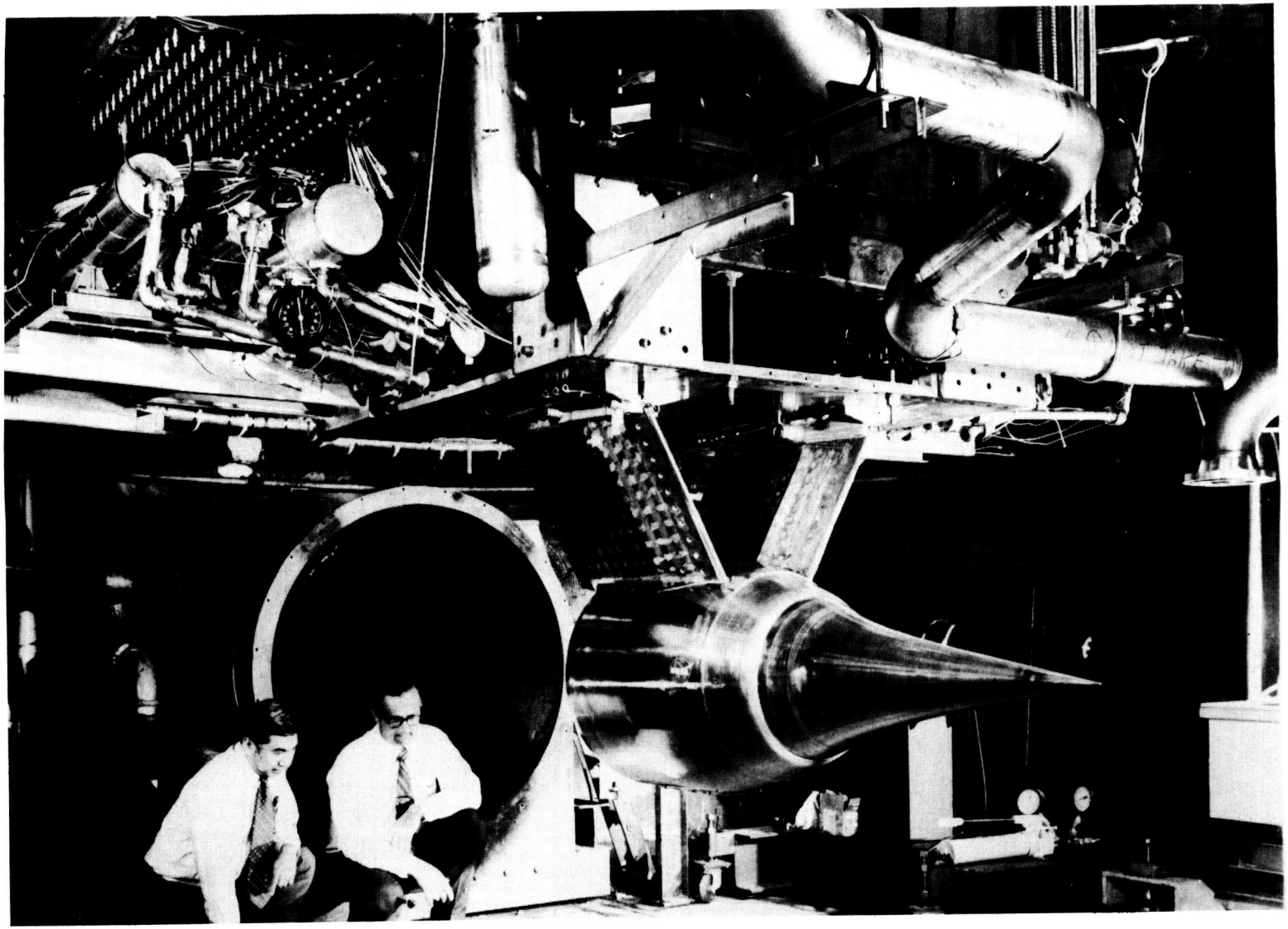

(c) AIM partially installed in Lewis hypersonic tunnel facility (HTF).

Figure 1.- Concluded.

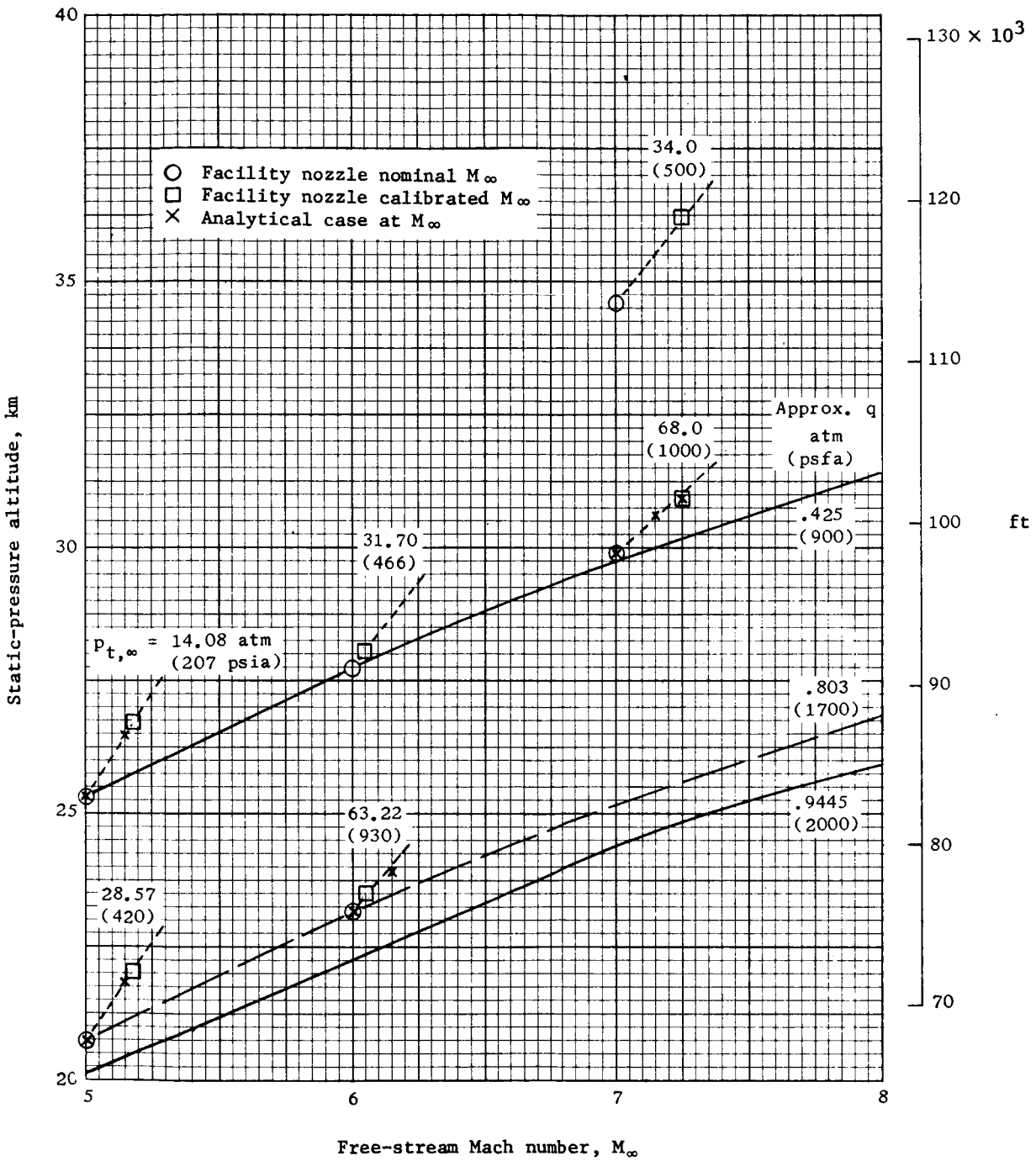


Figure 2.- Free-stream conditions. (Altitude values obtained by using static-pressure values corresponding to total pressures and Mach numbers in tables 2 and 3.)

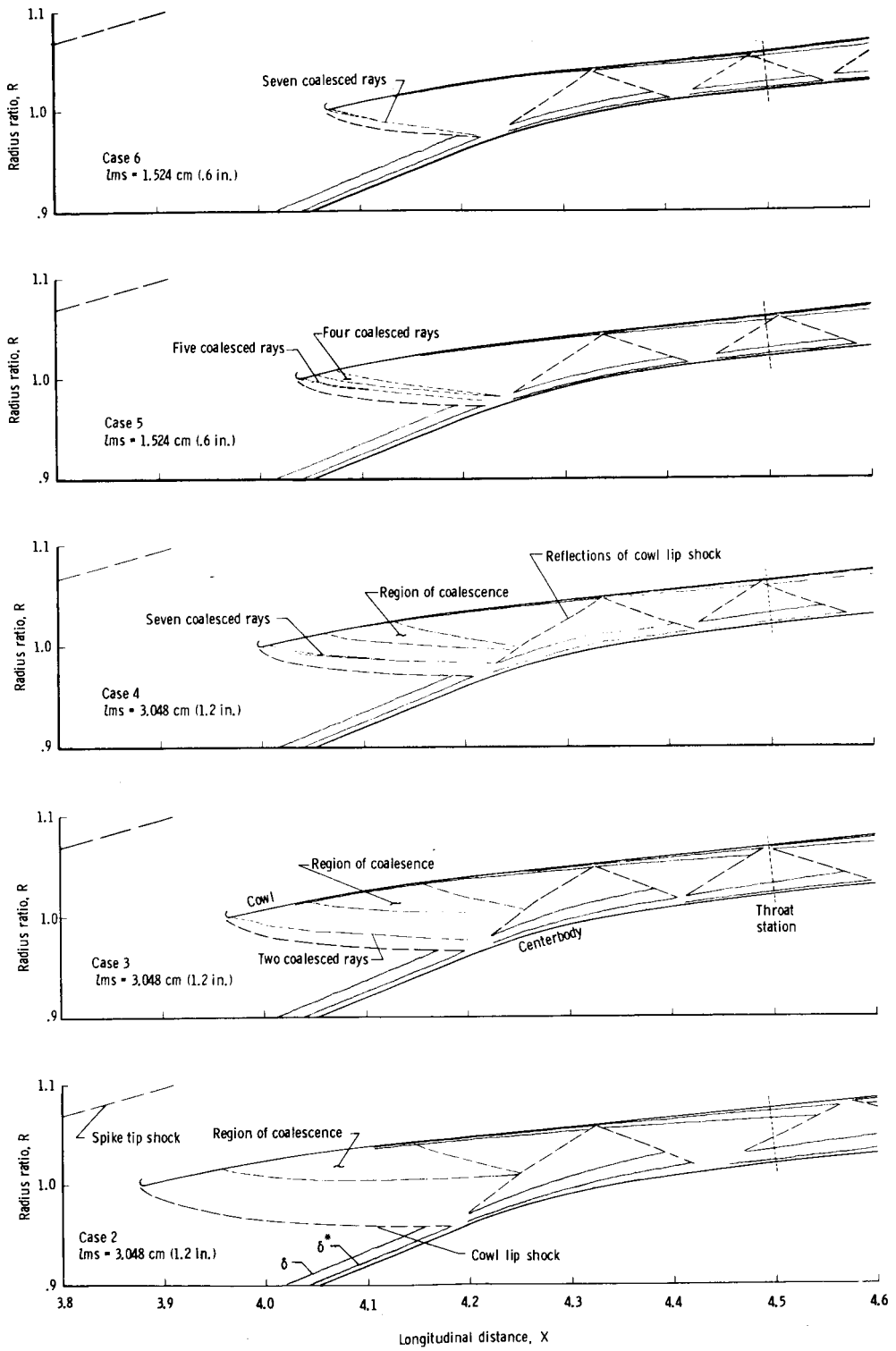


(a) Mach 5.0.

Figure 3.- Internal flow-field shock patterns for various cowl positions.

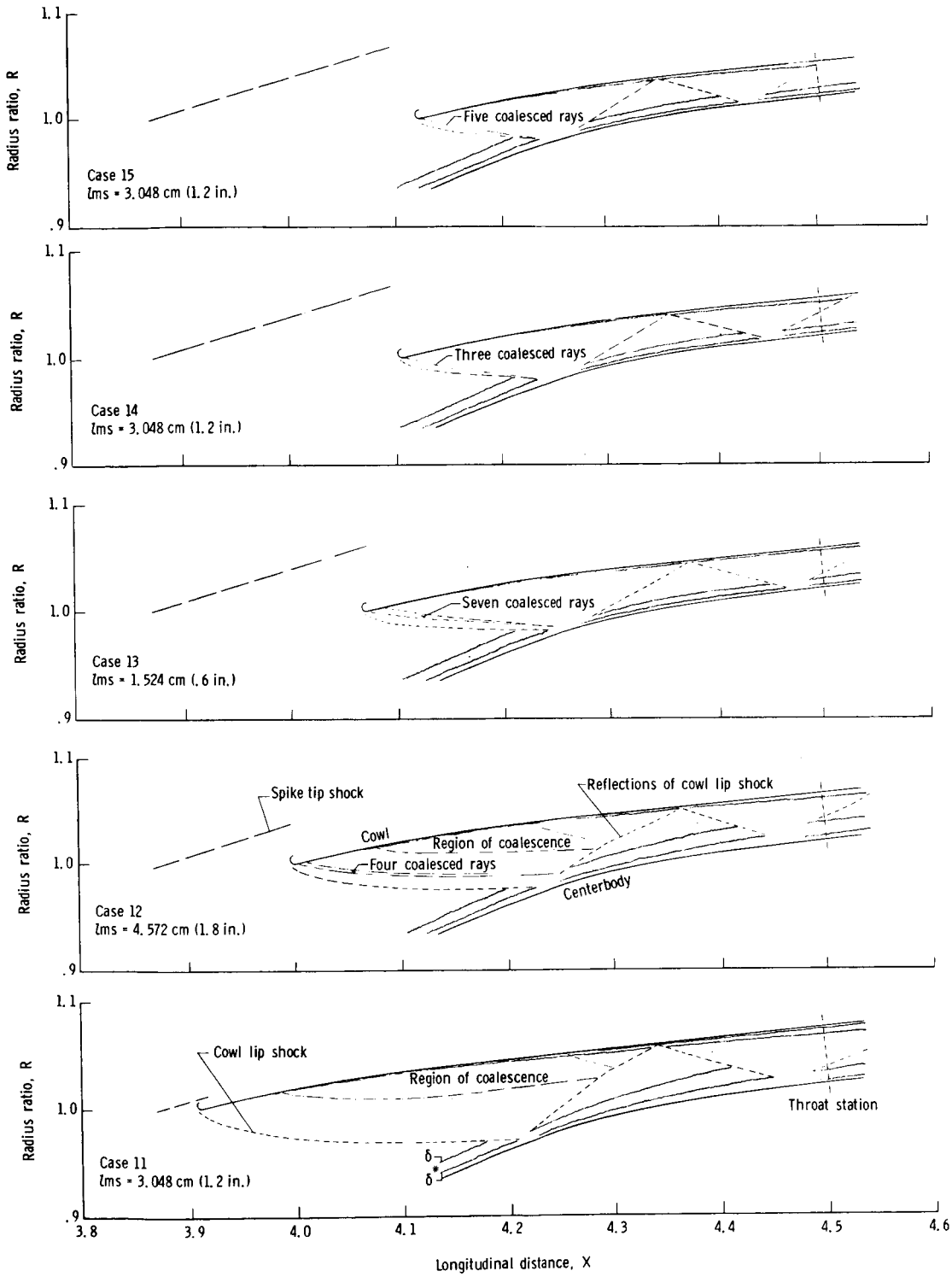


(b) Mach 6.0.

Figure 3.- Continued.

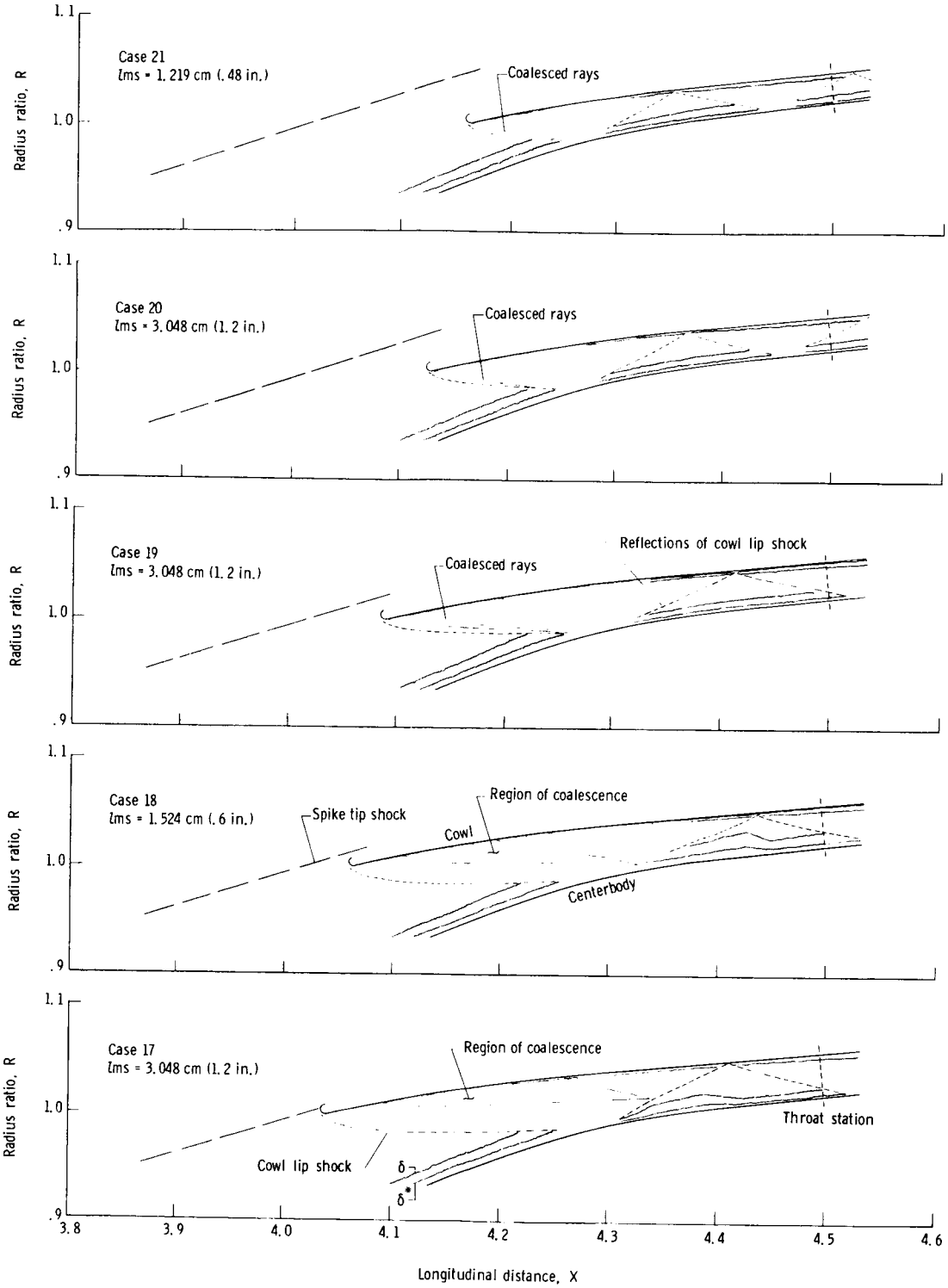


(c) Mach 7.0.

**Figure 3.- Concluded.**

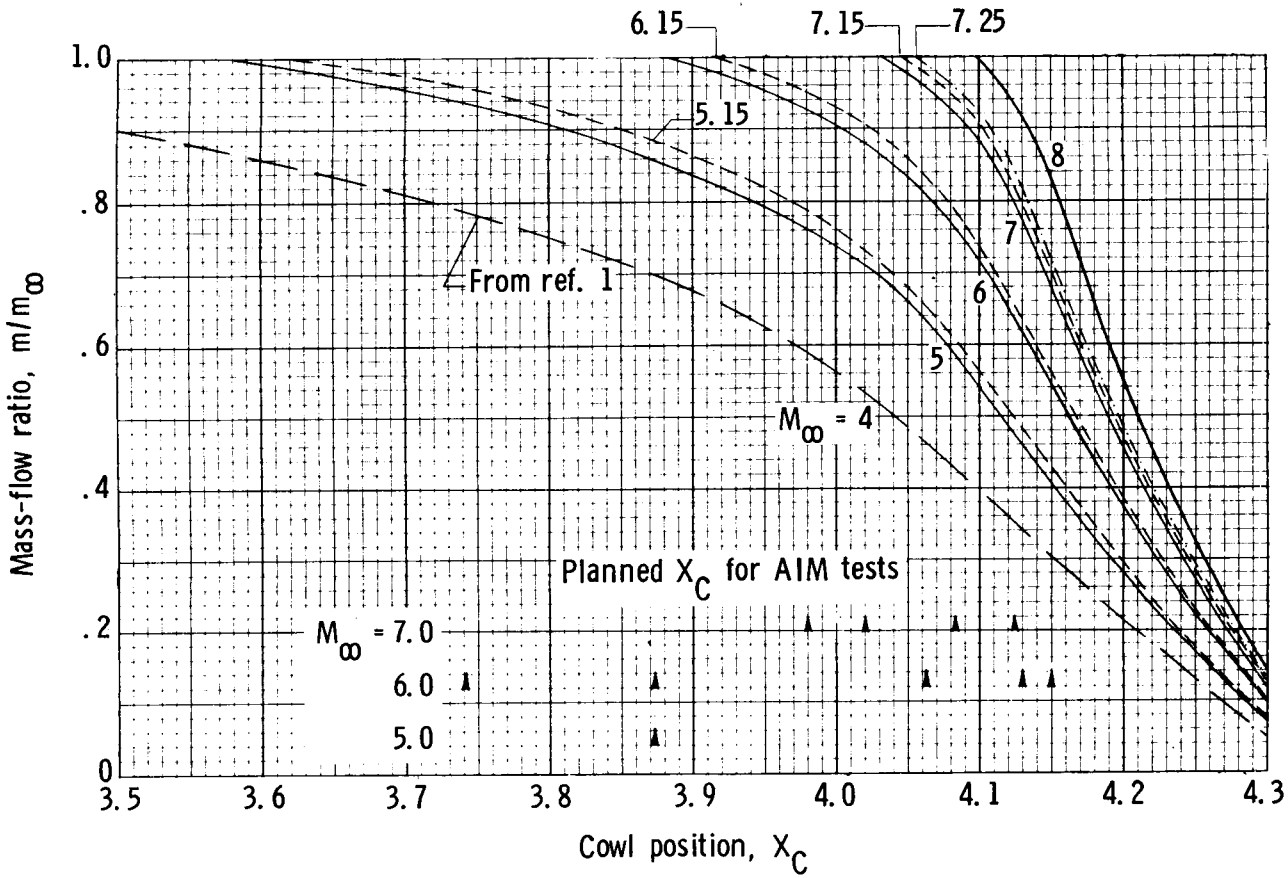


| M | $p_{t,\infty}$ atm | $T_{t,\infty}$ K |
|---|---|---|
| 4.0 | 11.43 | 880 |
| 5.0, 5.15 | 28.57 | 1225 |
| 6.0, 6.15 | 63.22 | 1628 |
| 7.0, 7.15, 7.25 | 68.00 | 2130 |
| 8.0 | 29.00 | 2583 |

(a) Mass-flow ratios. (Values defining most of the curves are given in table 5.)

Figure 4.- Mass-flow-ratio and additive-drag-coefficient schedules.

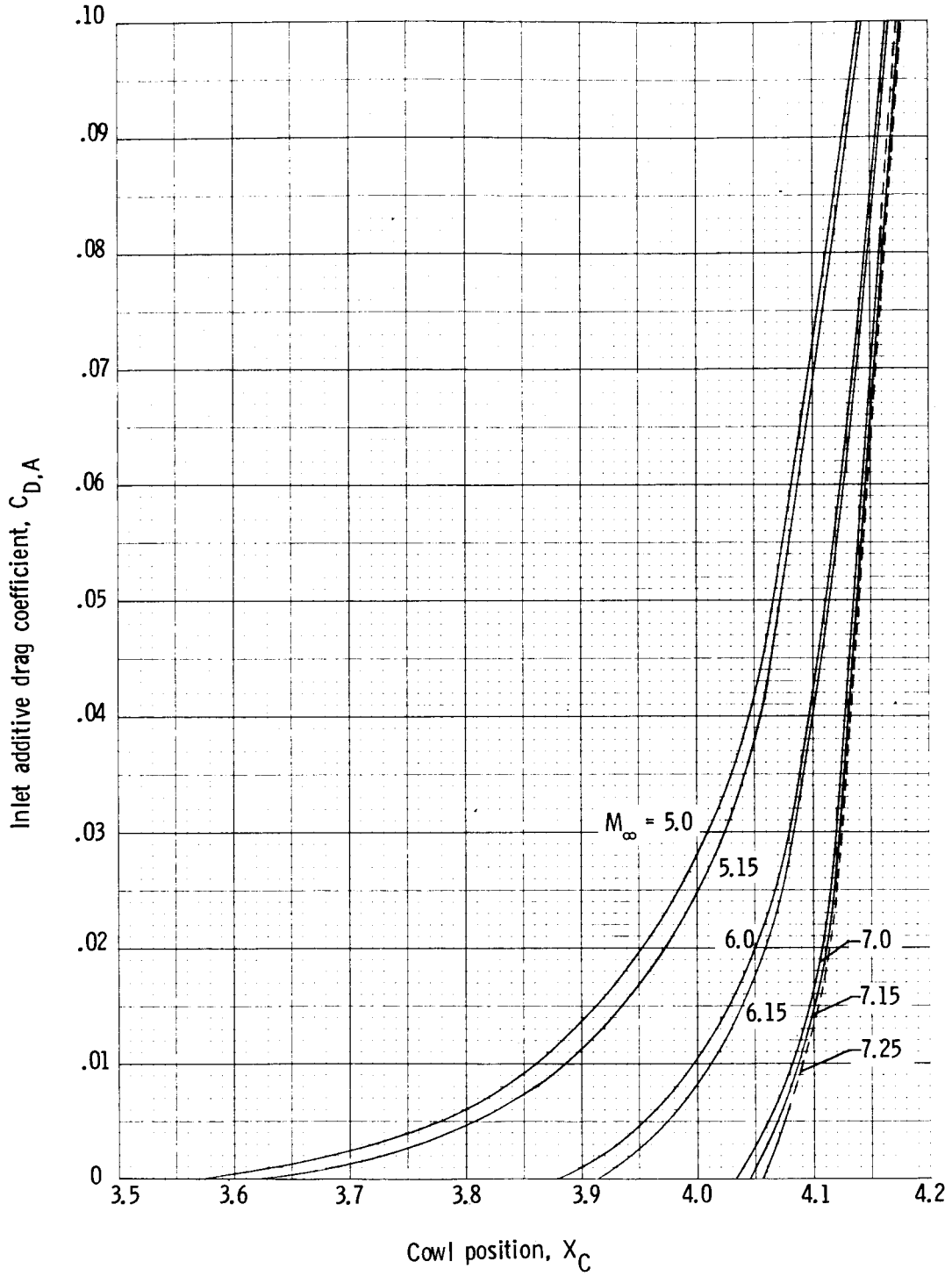


(b) Additive drag coefficients (dashed portion of curves are extrapolated). (Values defining curves are given in table 6.)

Figure 4.- Concluded.

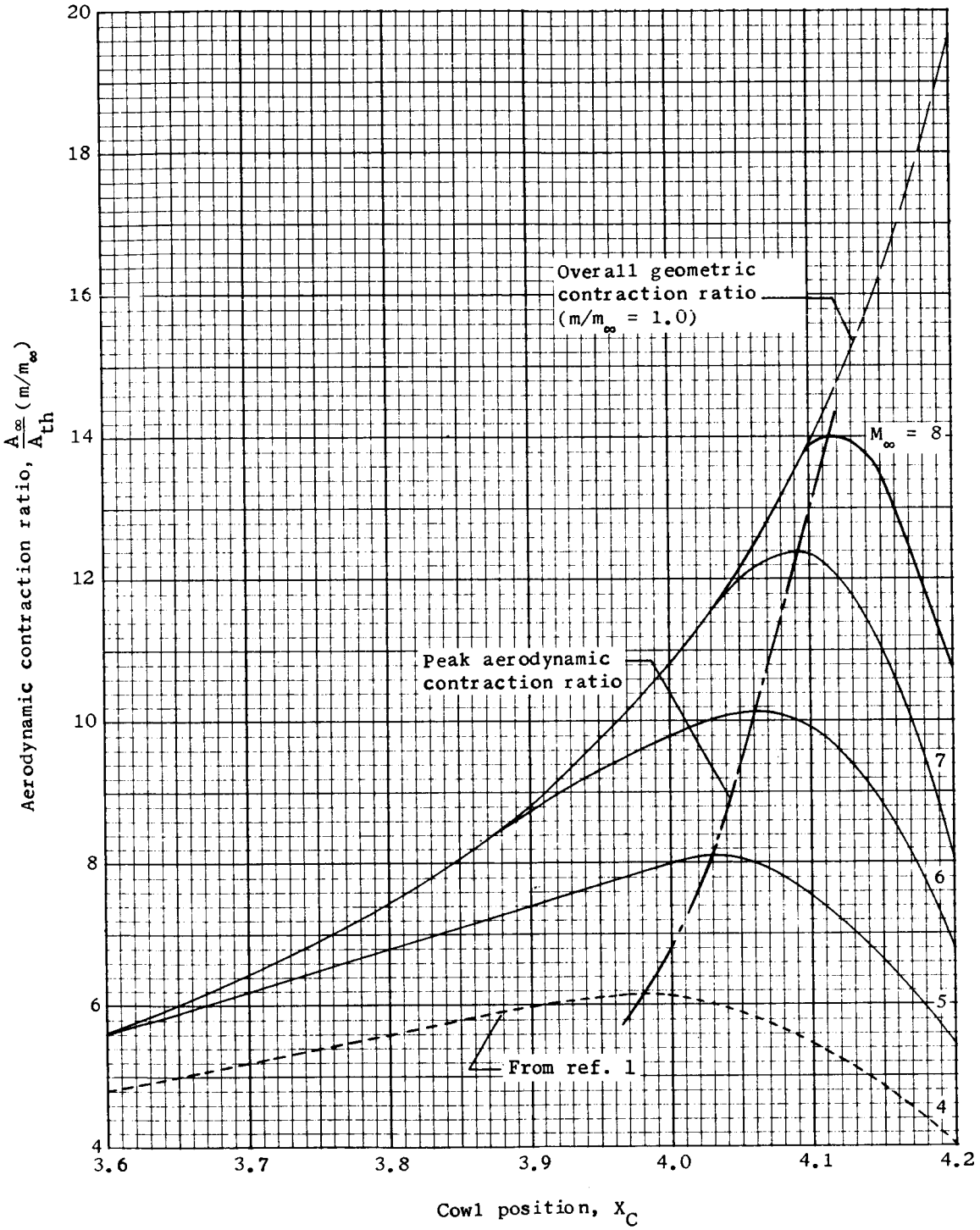


Figure 5.- Aerodynamic-contraction-ratio schedules.

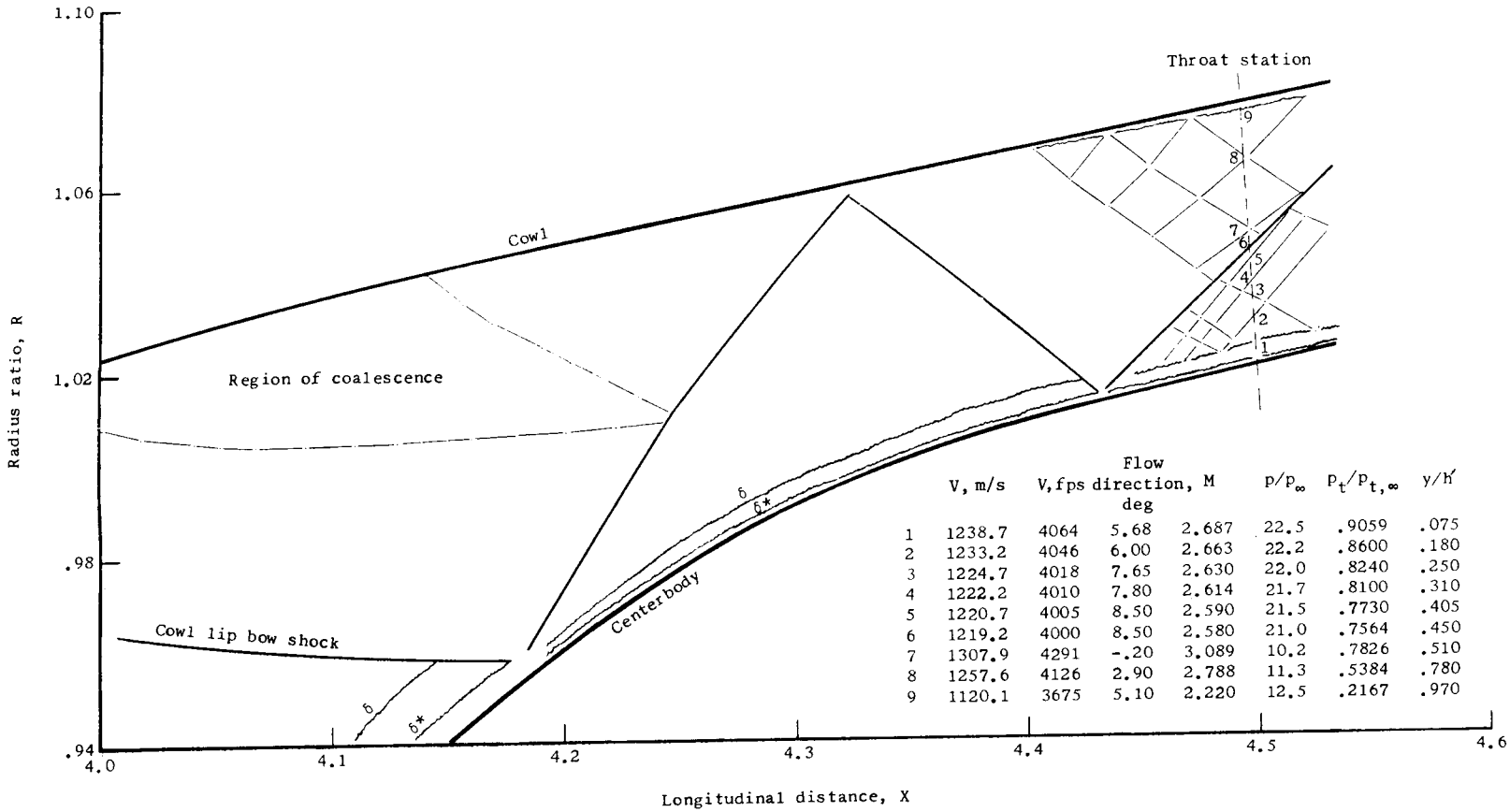


| | V, m/s | V, fps | Flow direction, deg | M | $p/p_\infty$ | $p_t/p_{t,\infty}$ | y/h' |
|---|---|---|---|---|---|---|---|
| 1 | 1238.7 | 4064 | 5.68 | 2.687 | 22.5 | .9059 | .075 |
| 2 | 1233.2 | 4046 | 6.00 | 2.663 | 22.2 | .8600 | .180 |
| 3 | 1224.7 | 4018 | 7.65 | 2.630 | 22.0 | .8240 | .250 |
| 4 | 1222.2 | 4010 | 7.80 | 2.614 | 21.7 | .8100 | .310 |
| 5 | 1220.7 | 4005 | 8.50 | 2.590 | 21.5 | .7730 | .405 |
| 6 | 1219.2 | 4000 | 8.50 | 2.580 | 21.0 | .7564 | .450 |
| 7 | 1307.9 | 4291 | -.20 | 3.089 | 10.2 | .7826 | .510 |
| 8 | 1257.6 | 4126 | 2.90 | 2.788 | 11.3 | .5384 | .780 |
| 9 | 1120.1 | 3675 | 5.10 | 2.220 | 12.5 | .2167 | .970 |

**Figure 6.- Typical internal flow field and conditions at the throat $M_\infty = 5.0$; $X_C = 0.8860$ m (2.90698 ft); $m/m_\infty = 0.8589$.**

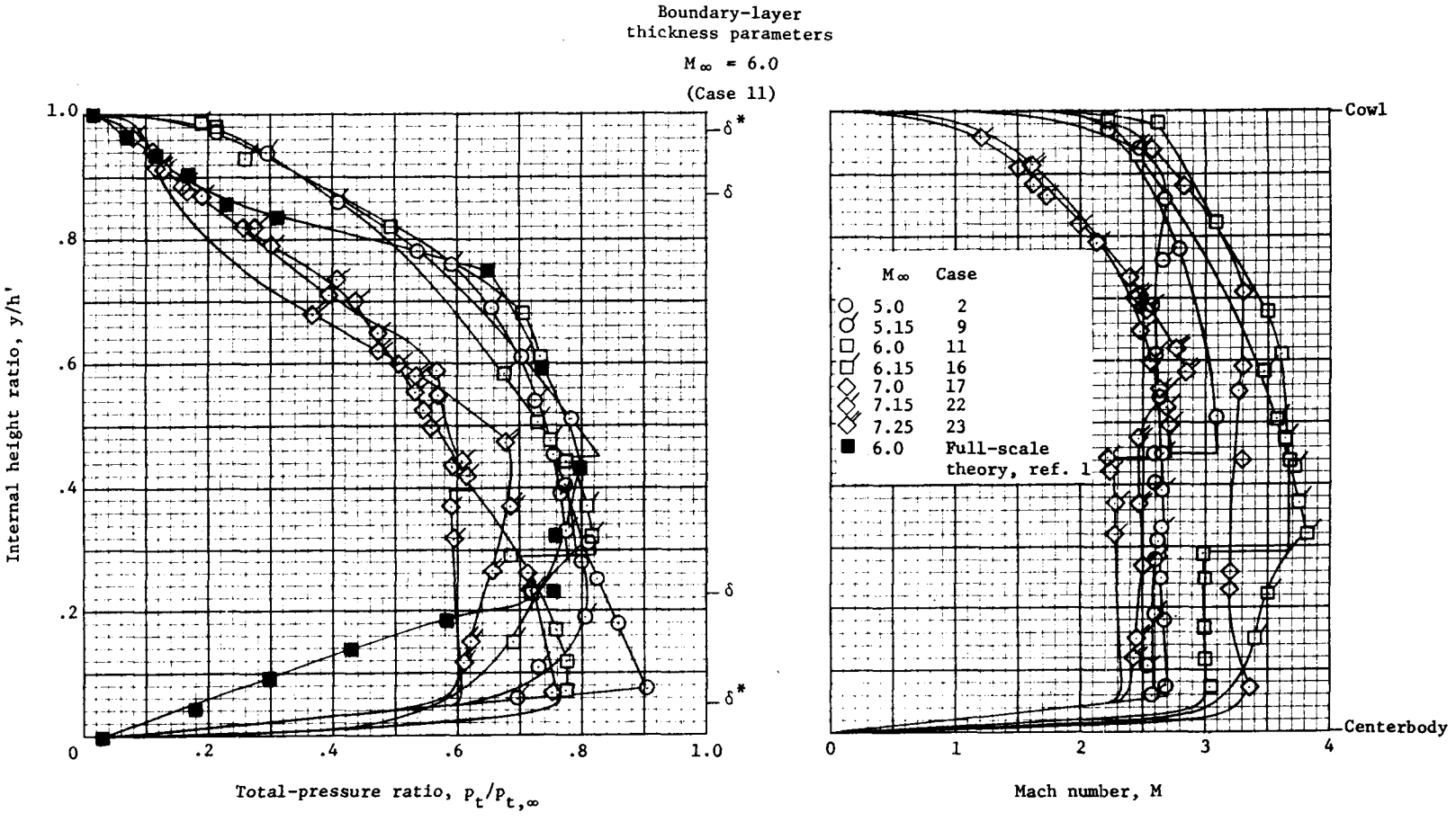


Figure 7.- Total-pressure recovery and Mach number profiles at throat station for operating cowl-centerbody configurations.

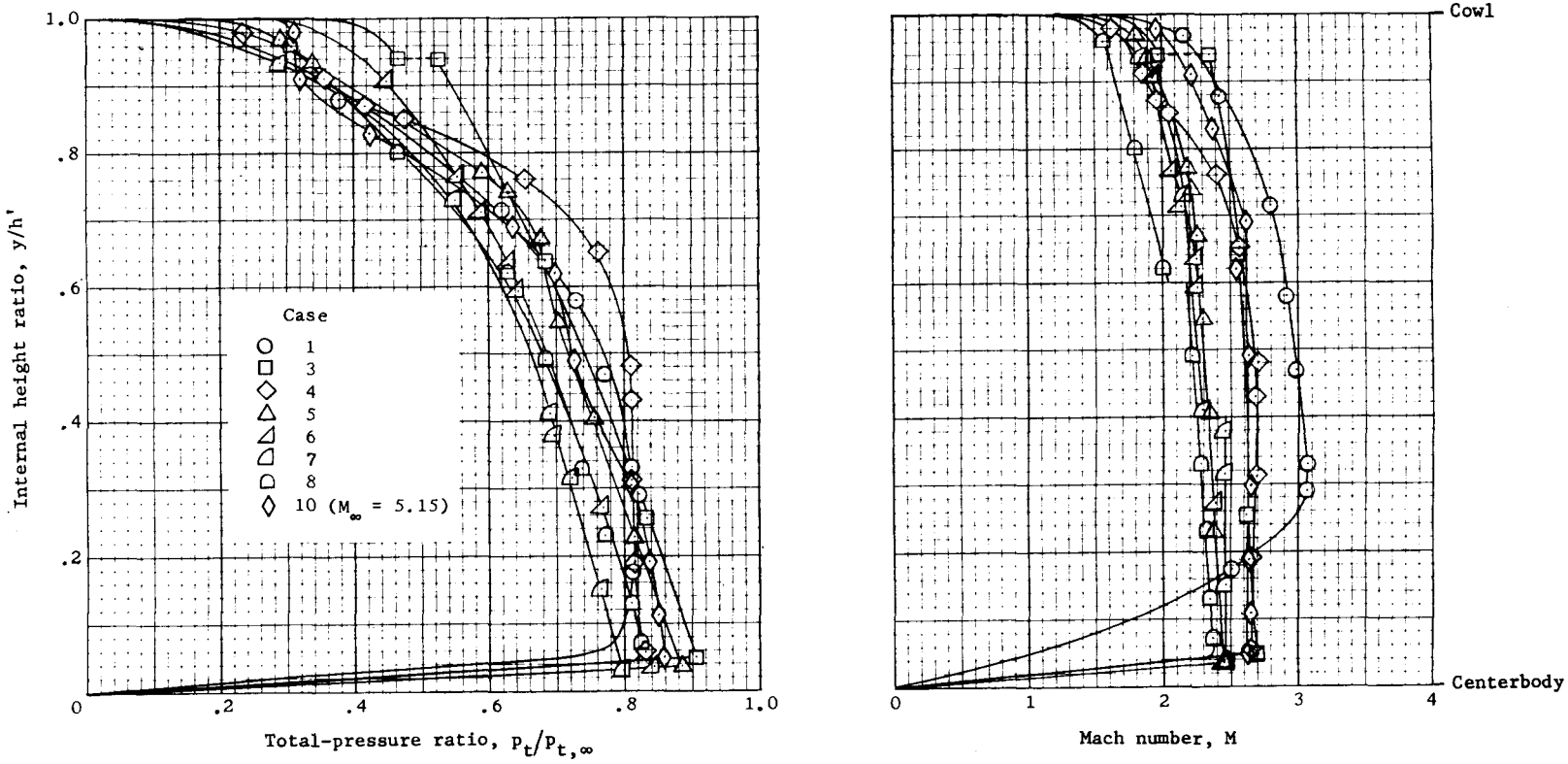


(a) $M_\infty = 5.0$.

Figure 8.- Total-pressure ratio and Mach number profiles at throat station for various cowl-centerbody positions.

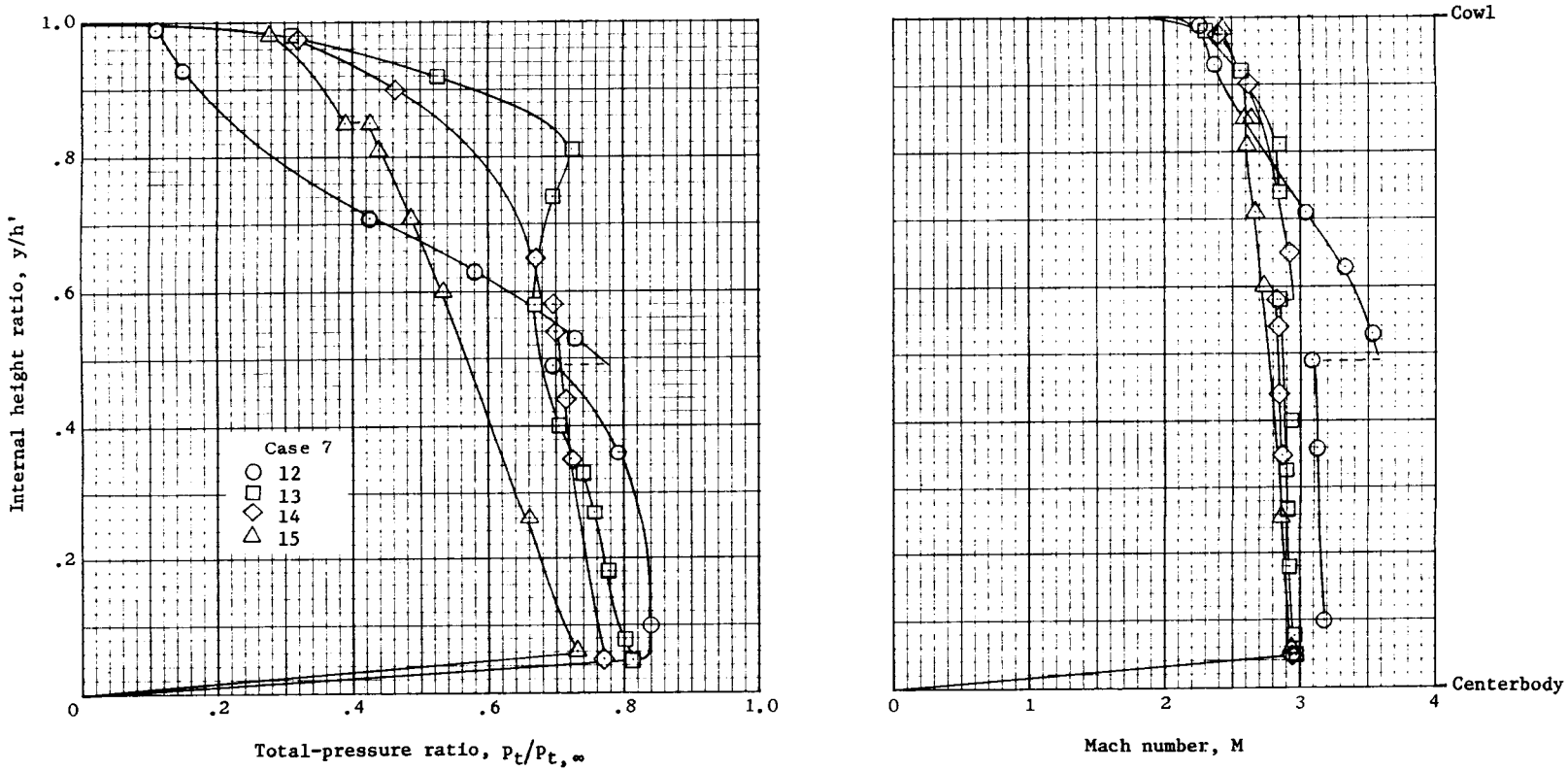


(b) $M_\infty = 6.0$.

Figure 8.- Continued.

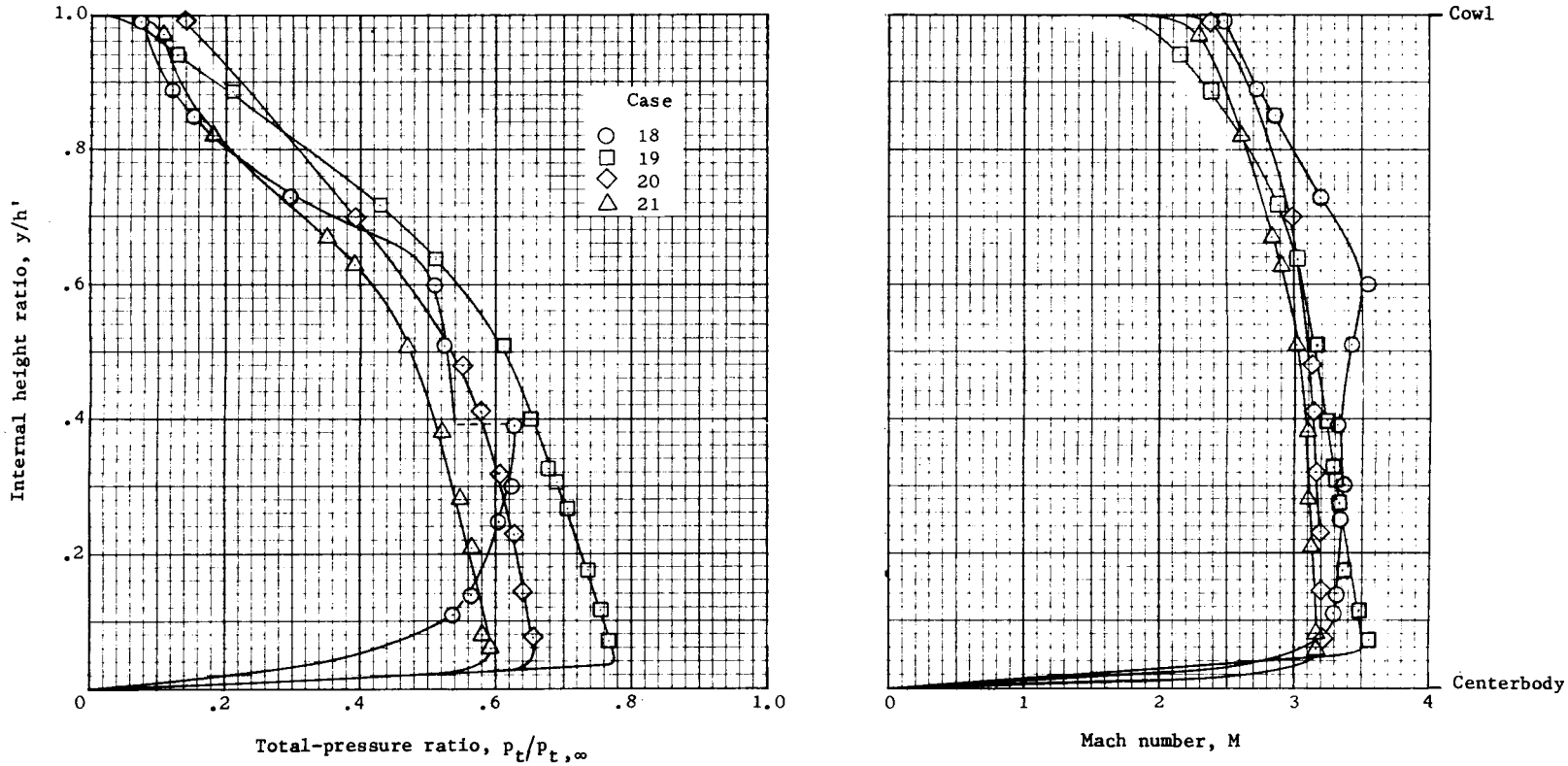


(c) $M_\infty = 7.0$.

Figure 8.- Concluded.

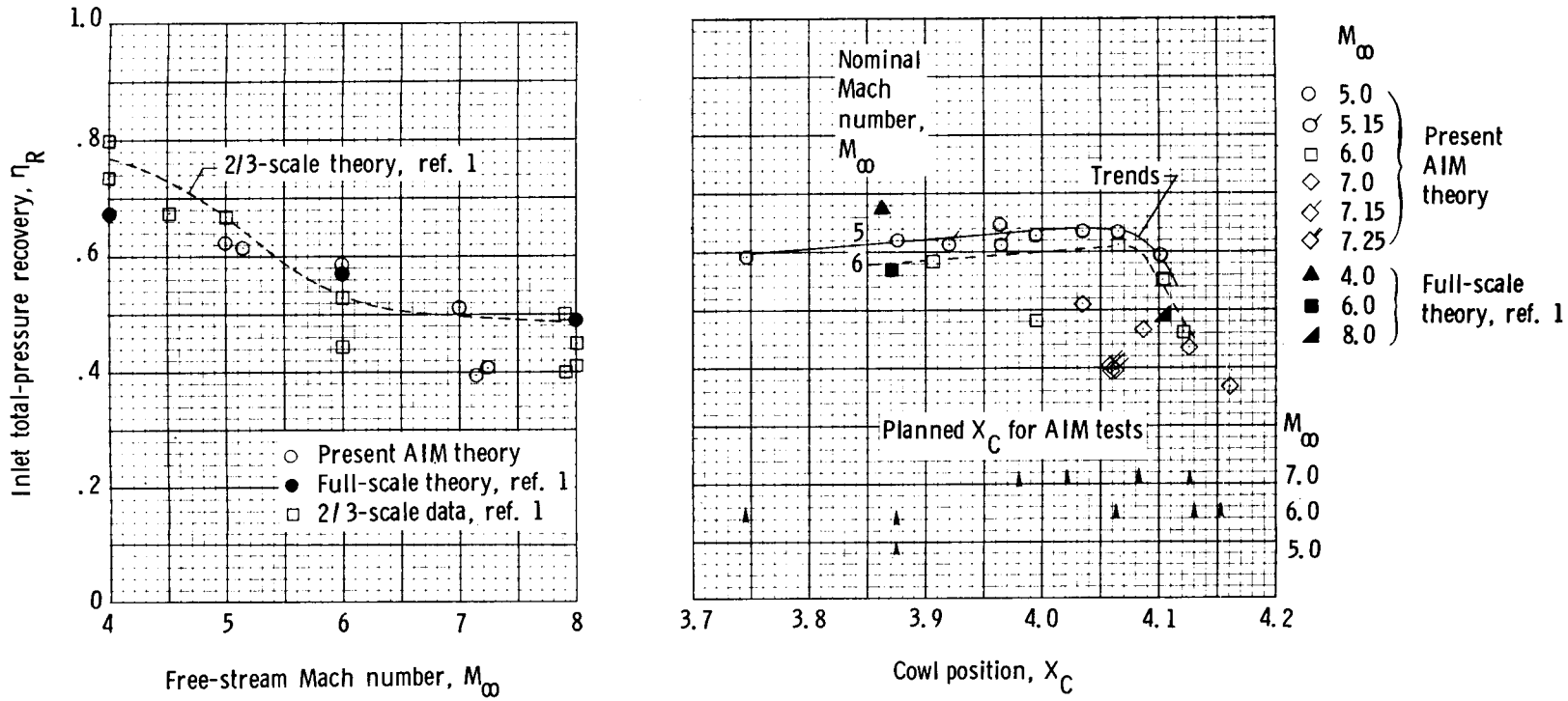


(a) Variation with free-stream Mach number.

(b) Variation with cowl position.

Figure 9.- Inlet mass-weighted average total-pressure recoveries.

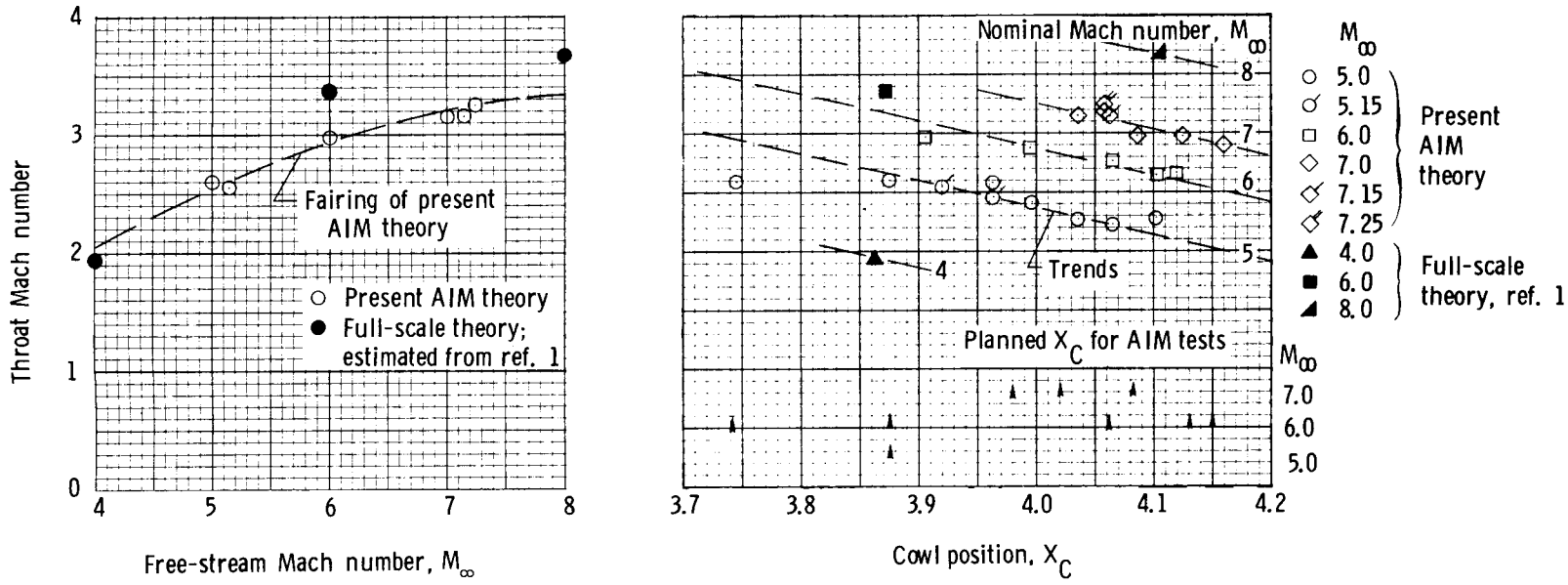


(a) Variation with free-stream Mach number.

(b) Variation with cowl position.

Figure 10.- Inlet mass-weighted average throat Mach numbers.

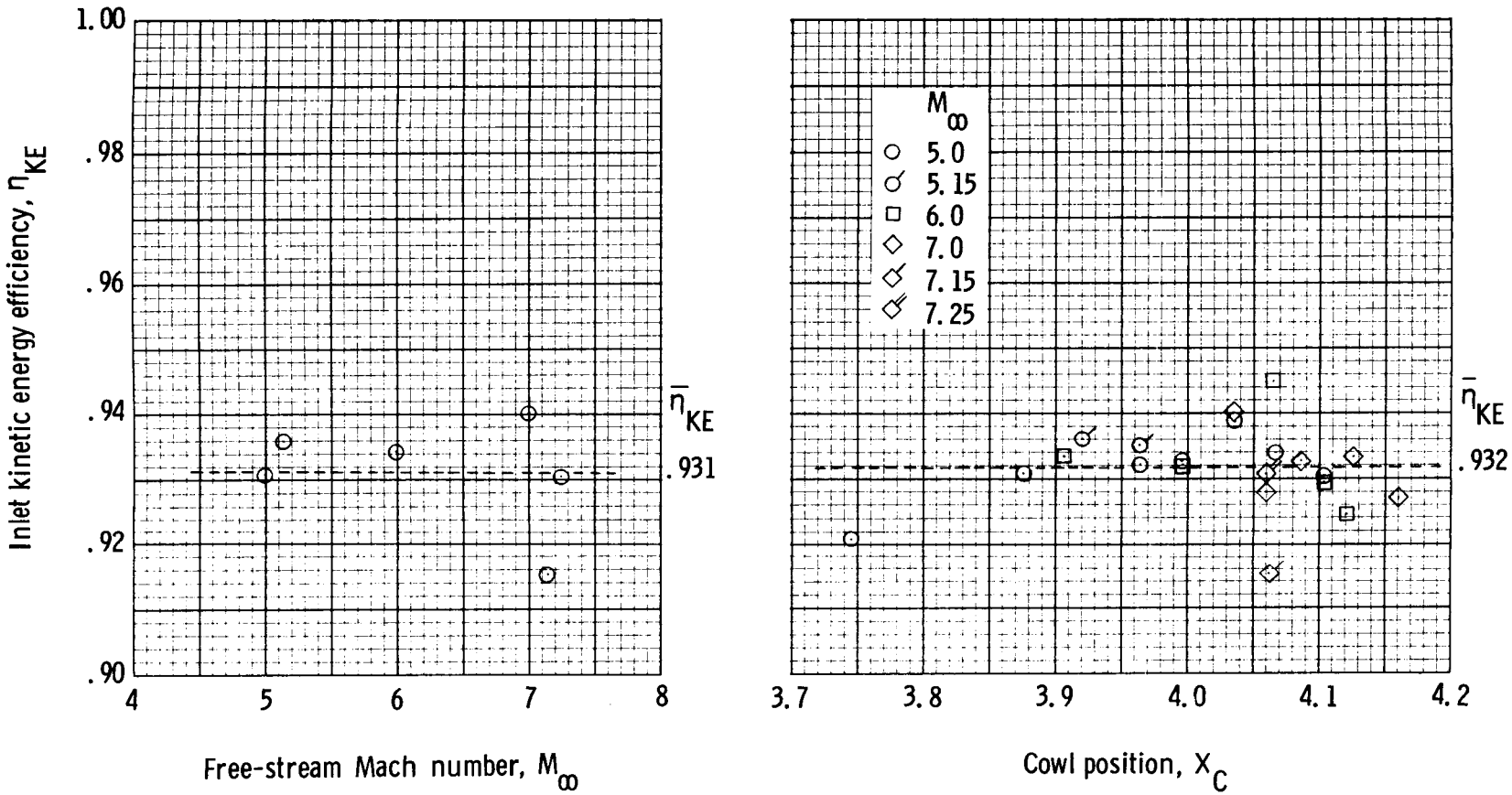


(a) Variation with free-stream Mach number.

(b) Variation with cowl position.

Figure 11.- Inlet mass-weighted average kinetic energy efficiencies, present AIM theory.

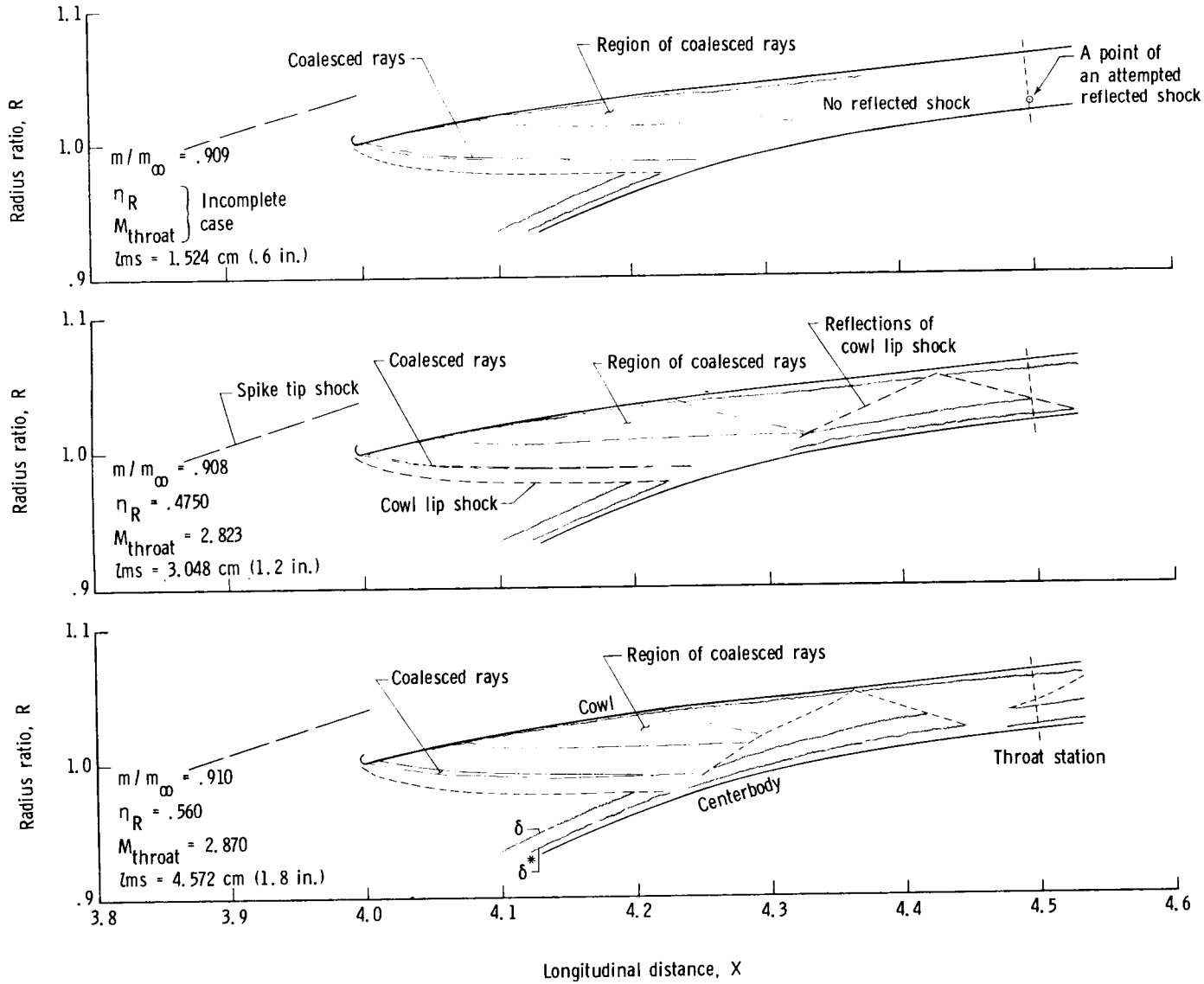


Figure 12.- Effects on internal flow of computer program sensitivities such as characteristic mesh size. $M_\infty = 6.0$; $X_C = 3.996$; case 12.